Exploring the subpolar to subtropical export pathways of the deep limb of the AMOC with tracers and simulated Lagrangian particles

Stefan Gary and Susan Lozier, Duke University

2nd Annual US AMOC Meeting, June 9, 2010, Miami, FL

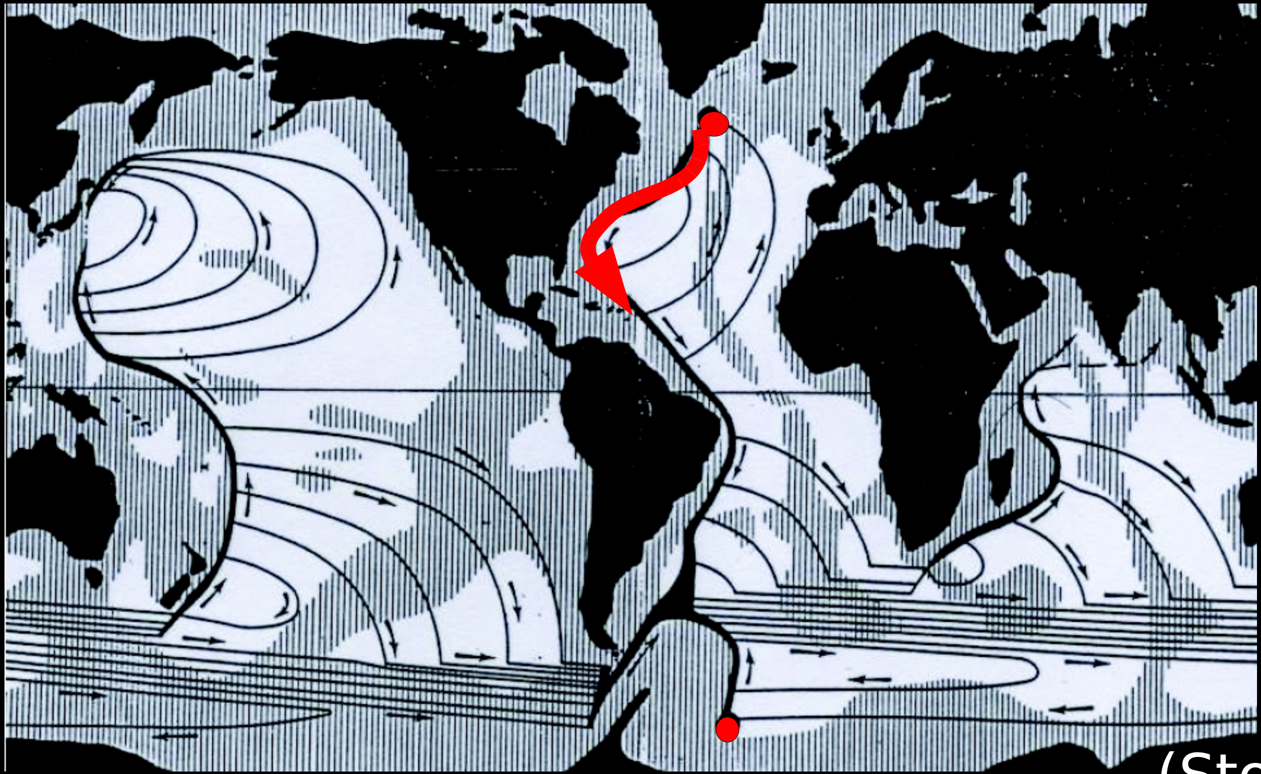

(Stommel, 1958)

Exploring the
subpolar to subtropical export pathways
of the
deep limb of the AMOC
with
tracers and simulated Lagrangian particles

Stefan Gary and Susan Lozier, Duke University

2nd Annual US AMOC Meeting, June 9, 2010, Miami, FL

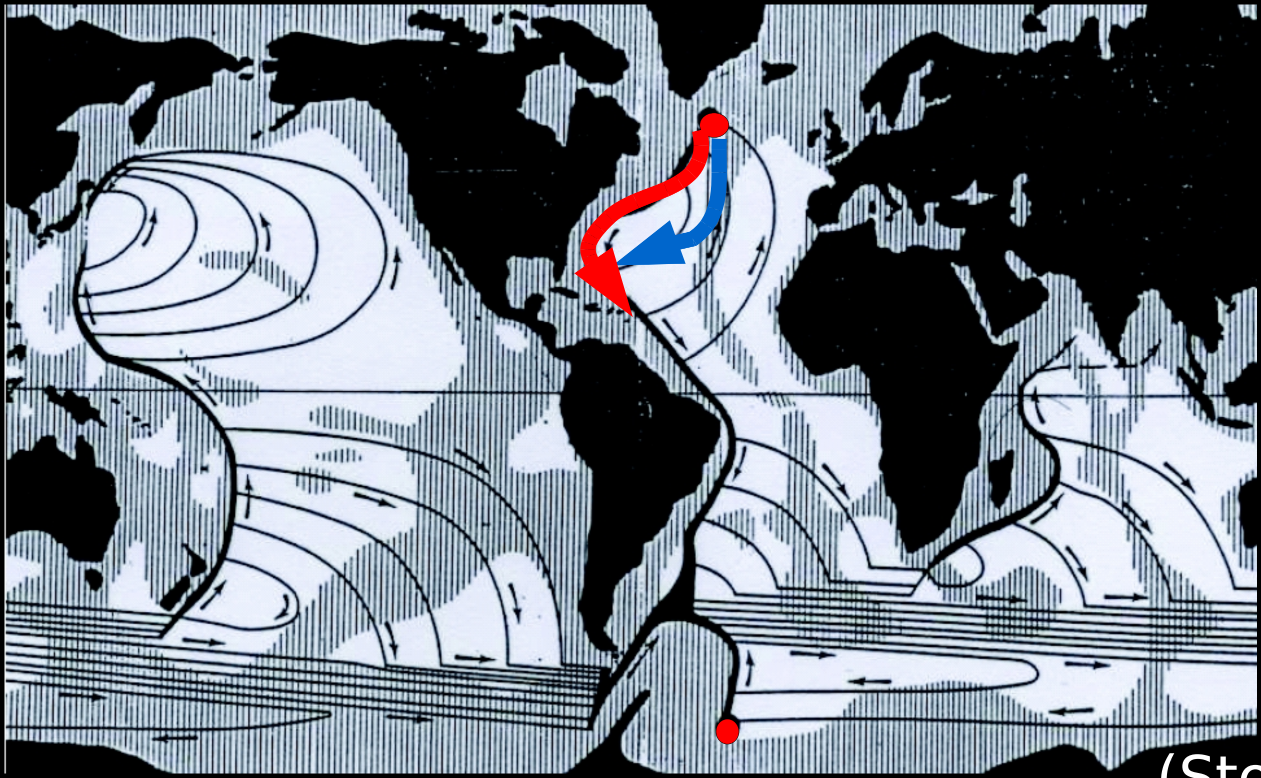

(Stommel, 1958)

Observations: DWBC & Interior Pathway

(1) The DWBC is a stable, equatorward current with higher velocities than the basin interior

(Schott et al. 2004, 2006, Watts, 1990).

CFC-11 concentrations are higher in the DWBC than the basin interior

(Smethie et al., 2000, Doney & Jenkins, 1994, Smethie, 1993).

(2) Most floats in the DWBC in the subpolar gyre exit before reaching the subtropics.

(Bower et al., 2009, Fischer & Schott, 2002, Lavender et al. 2000)

My goal is to resolve these seemingly contradictory observations.

Data Sources

Hydrographic and CFC-11 observations

- CARINA v1.0 (CARINA group, 2009)
- GLODAP v1.1 (Key et al. 2004)
- TTO-NAS leg 7 (J. Bullister & T. Tanhua, personal comm.)
- WHOI Line W (J. Toole et al., downloaded May 2010)
- WOD09 (NODC, downloaded April 2010)

ORCA025: 1/4° resolution, global z-coordinate model

(Barnier et al. 2006, Böning & Biastoch, personal communication)

- CORE hindcast forcing, 1958-2004 (Large & Yeager, 2004)
- Output: velocity, temperature, salinity, CFC-11
- Initial conditions: all zero
- Restoring: polar regions only, weak surface damping
- Trajectories calculated with ARIANE (Blanke & Grima, 2010)

Observed and modeled CFC-11 at 70°W

CARINA #69, Oct-Nov 2003

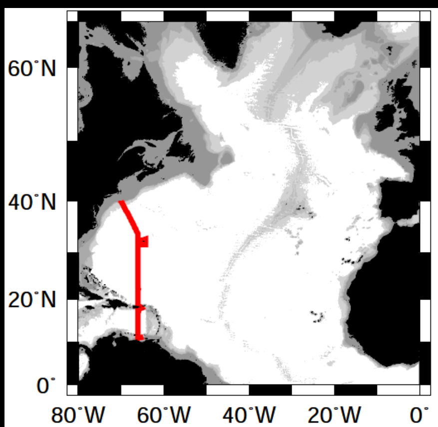

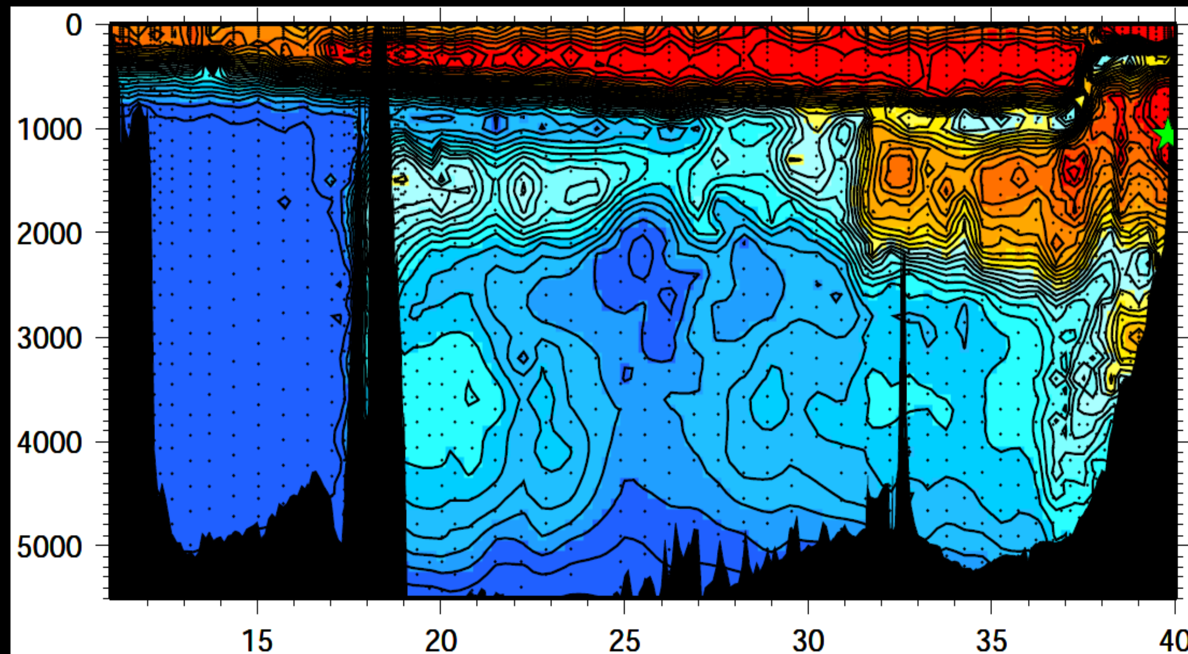

ORCA025, Nov. mean 2003

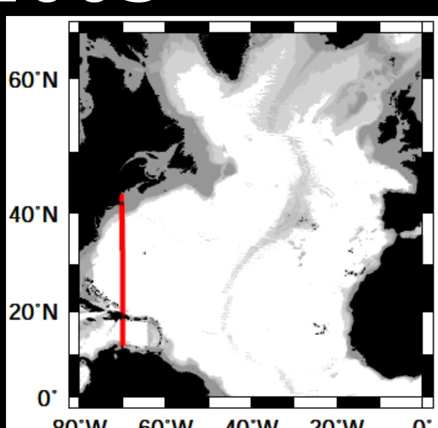

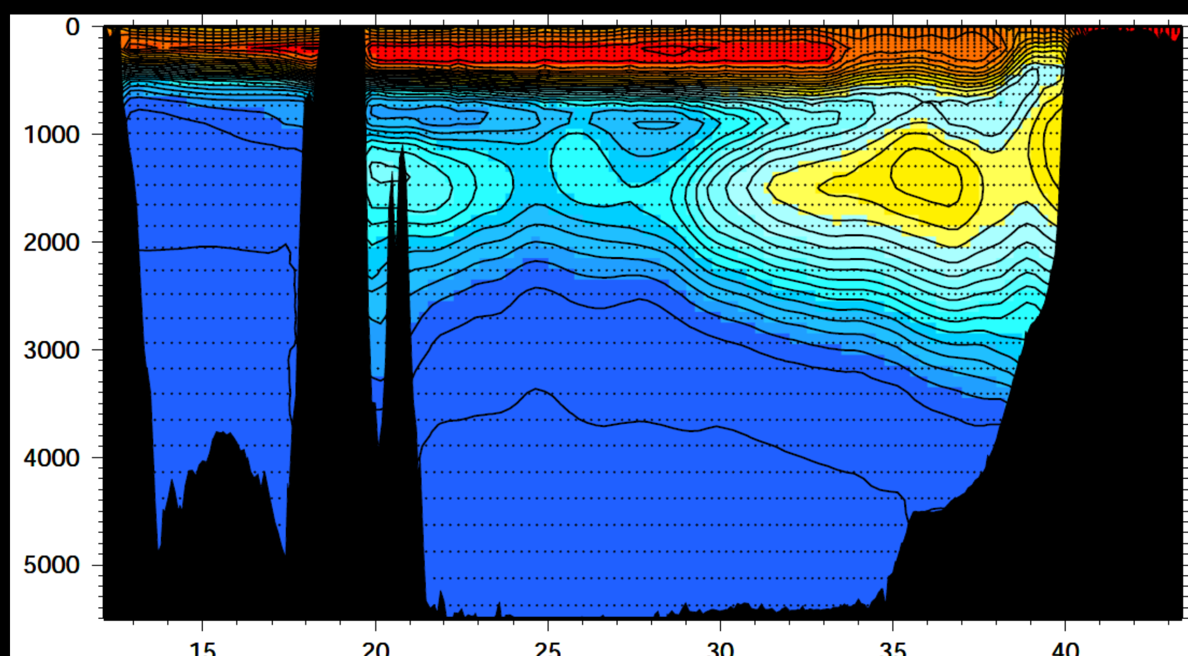

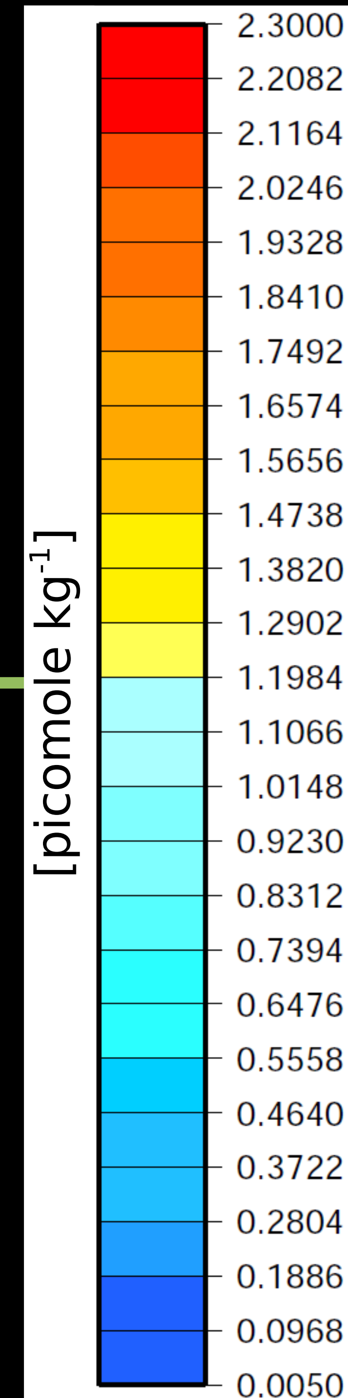

Connectivity of the tracer signal

CFC-11 max inshore 4000m & below 1000m

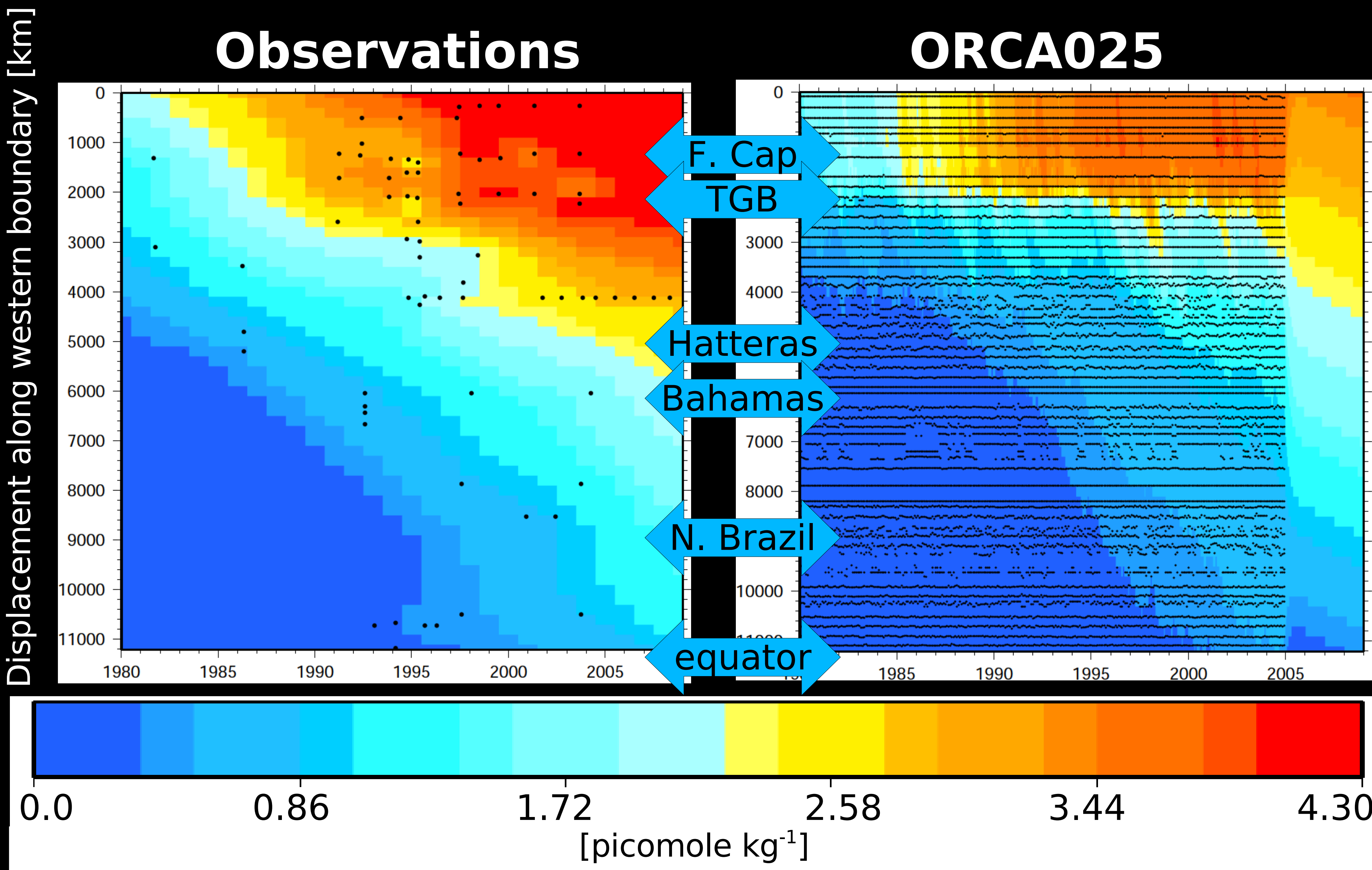

Connectivity of the tracer signal

CFC-11 max inshore 4000m & below 1000m

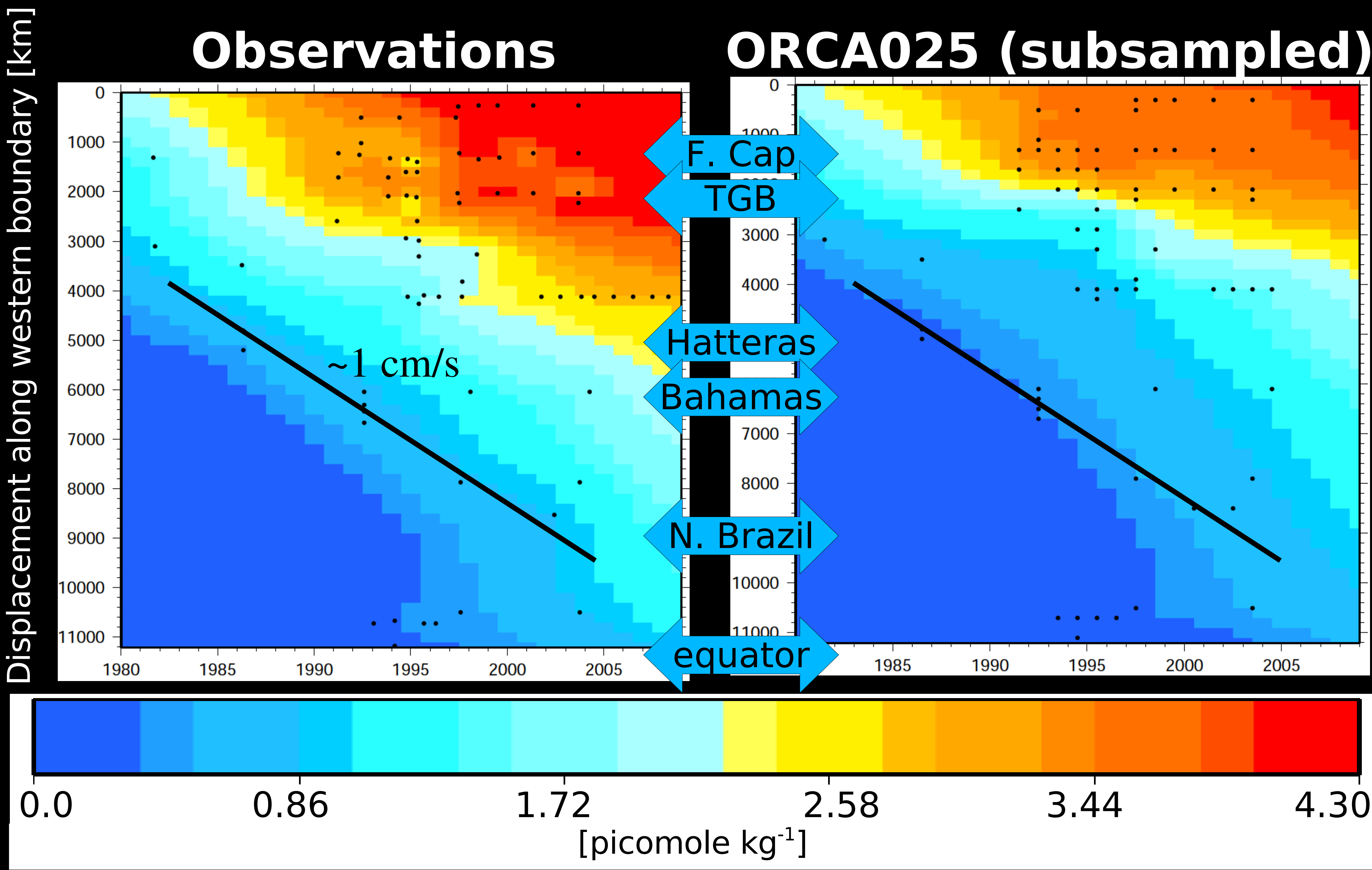

Lagrangian Pathways and Tracer

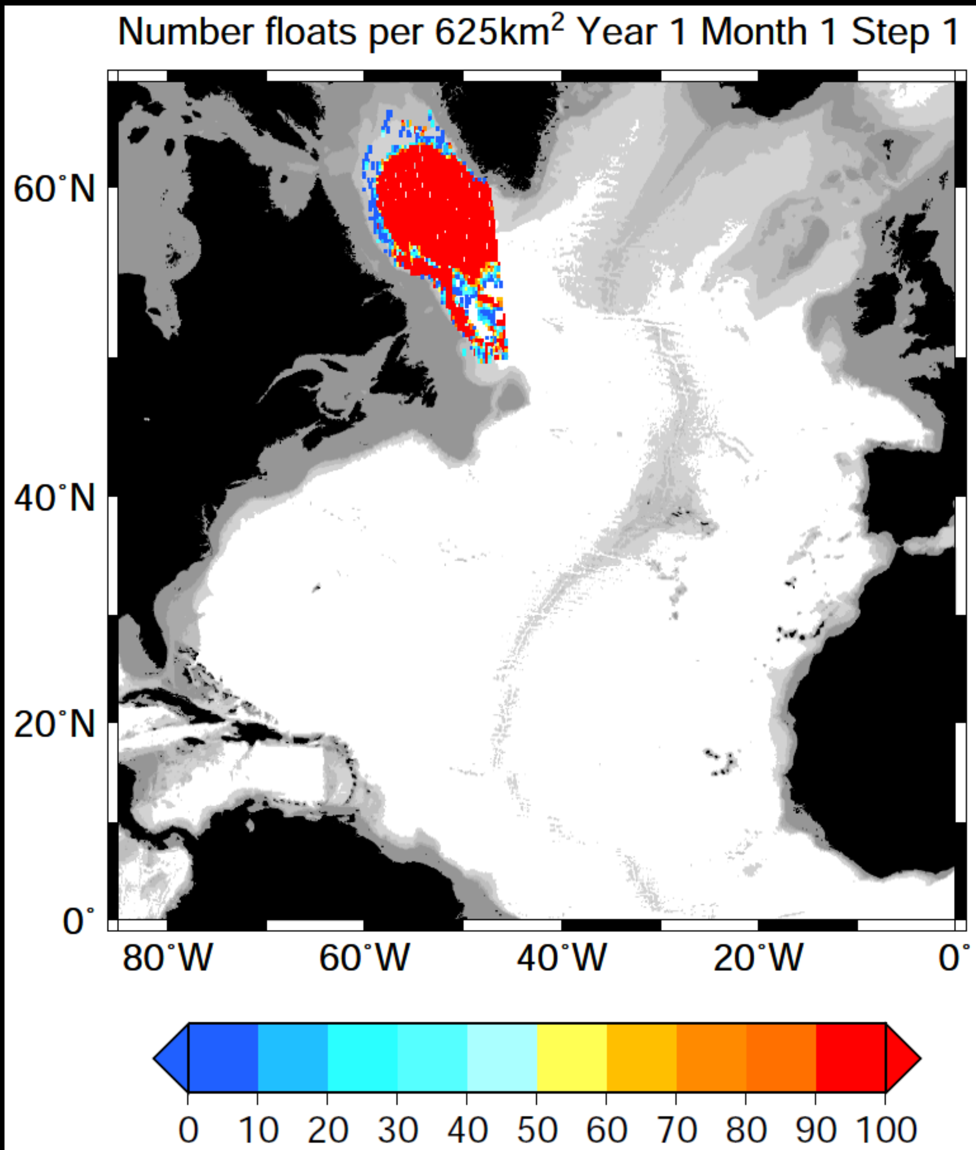

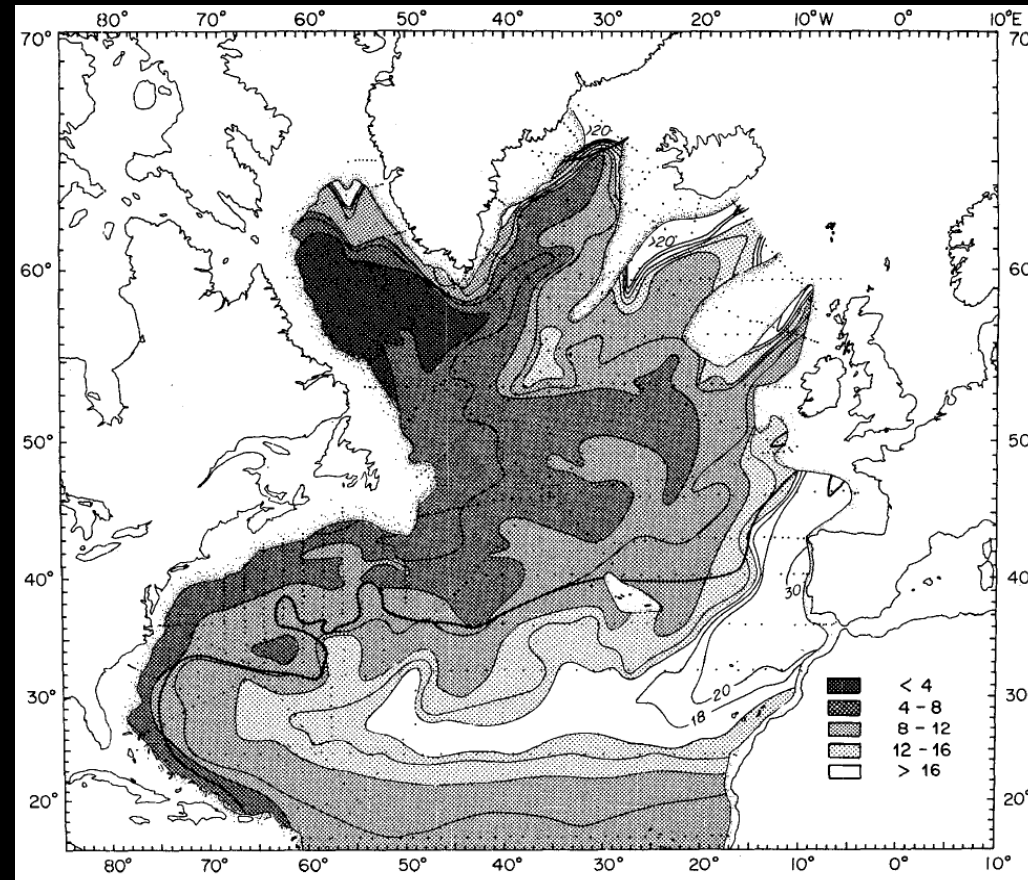

FIG. 3. Potential vorticity $(f/\rho)(\delta\rho/\delta z)$, in units of 10^{-14} cm^{-1} s^{-1}, at the LSW potential vorticity minimum, using the data of Fig. 1 The potential vorticity is a local measure of the vertical homogeneity of the water mass. The heavy curves are the limits of the identifiabl LSW potential vorticity minimum. Beyond these curves, contouring is continued on the σ_{1500} = 34.72 mg cm^{-3} surface. Contou intervals are 2×10^{-14} cm^{-1} s^{-1}.

(Talley & McCartney, 1982)

9.7×10^5 Lagrangian particles launched below 1000m at potential vorticities < 3×10^{-12} m^{-1}s^{-1}. Trajectories were integrated in the repeated, 5-day mean 1990 - 2004 ORCA025 velocity fields for 50 years.

Lagrangian Pathways and Tracer

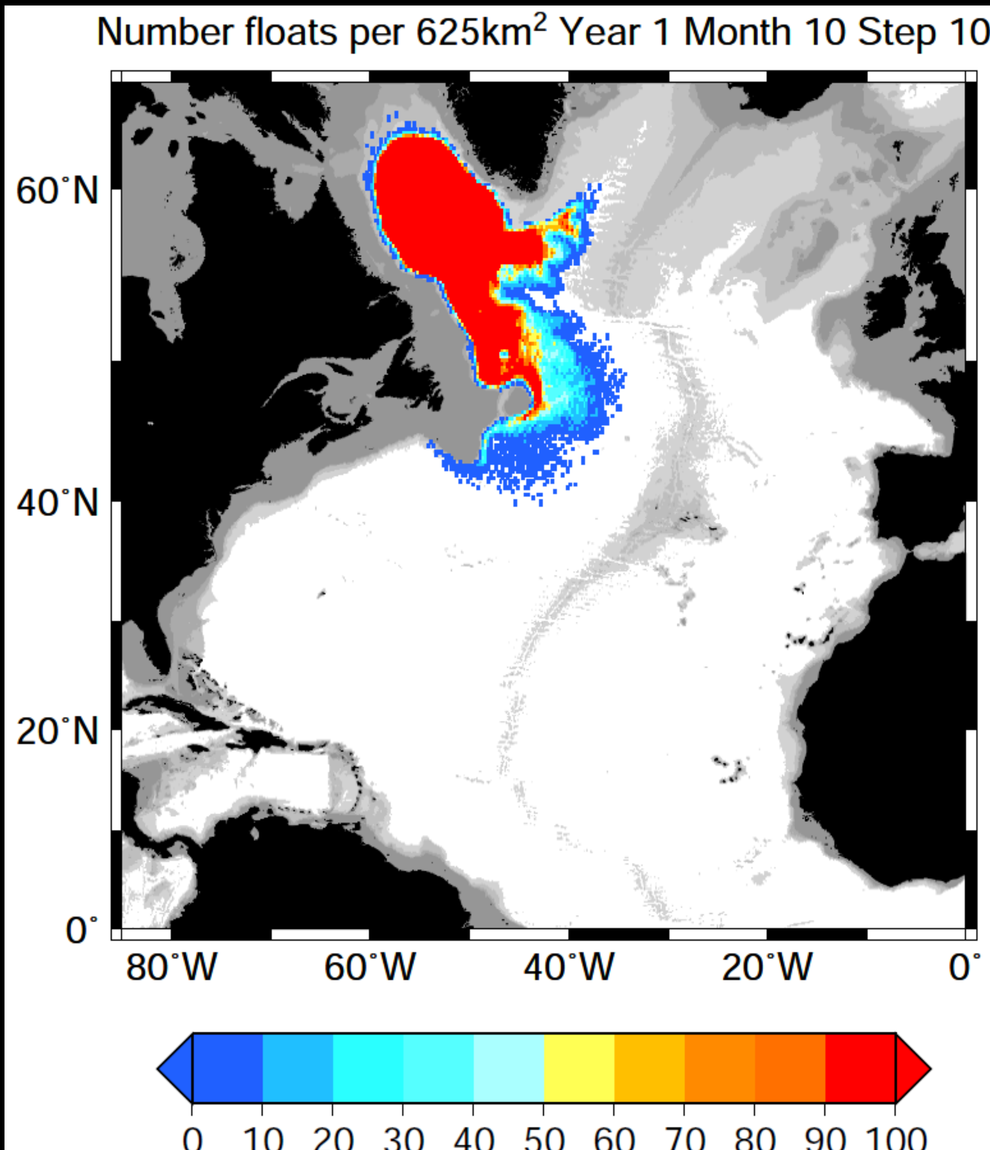

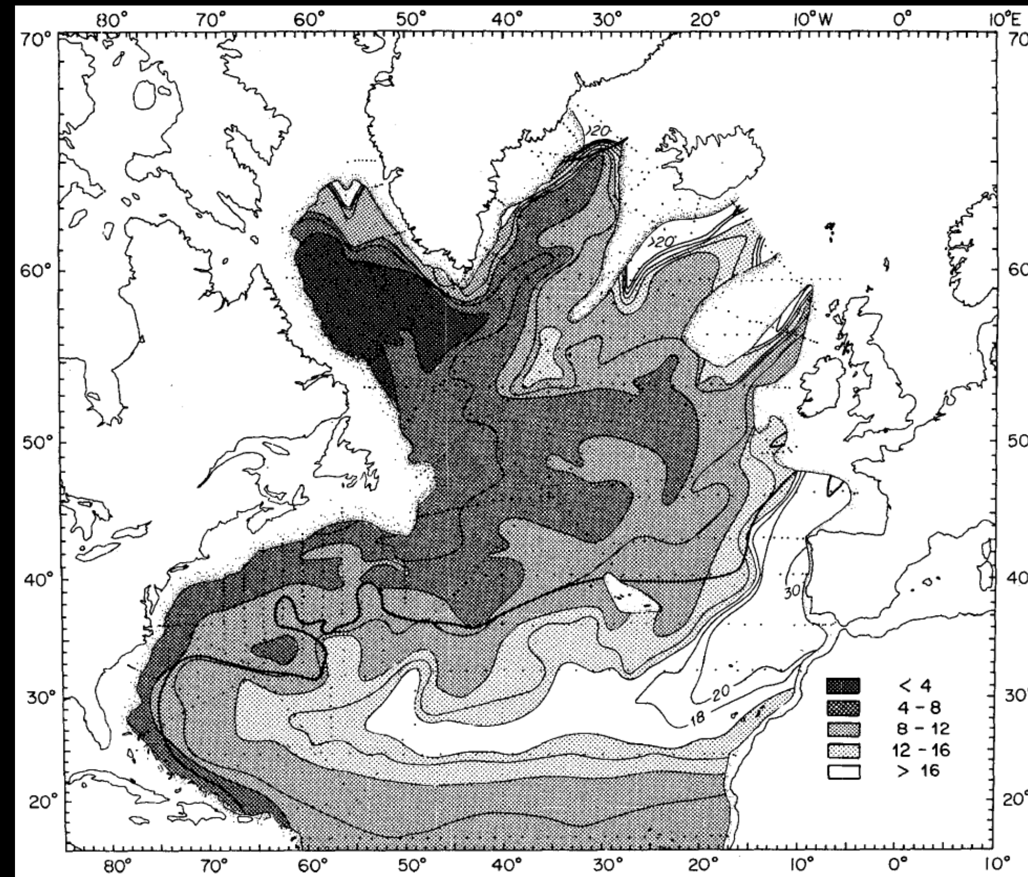

FIG. 3. Potential vorticity $(f/\rho)(\delta\rho/\delta z)$, in units of 10^{-14} cm^{-1} s^{-1}, at the LSW potential vorticity minimum, using the data of Fig. 1. The potential vorticity is a local measure of the vertical homogeneity of the water mass. The heavy curves are the limits of the identifiable LSW potential vorticity minimum. Beyond these curves, contouring is continued on the σ_{1500} = 34.72 mg cm^{-3} surface. Contour intervals are 2×10^{-14} cm^{-1} s^{-1}.

(Talley & McCartney, 1982)

9.7×10^5 Lagrangian particles launched below 1000m at potential vorticities < 3×10^{-12} m^{-1}s^{-1}. Trajectories were integrated in the repeated, 5-day mean 1990 - 2004 ORCA025 velocity fields for 50 years.

Lagrangian Pathways and Tracer

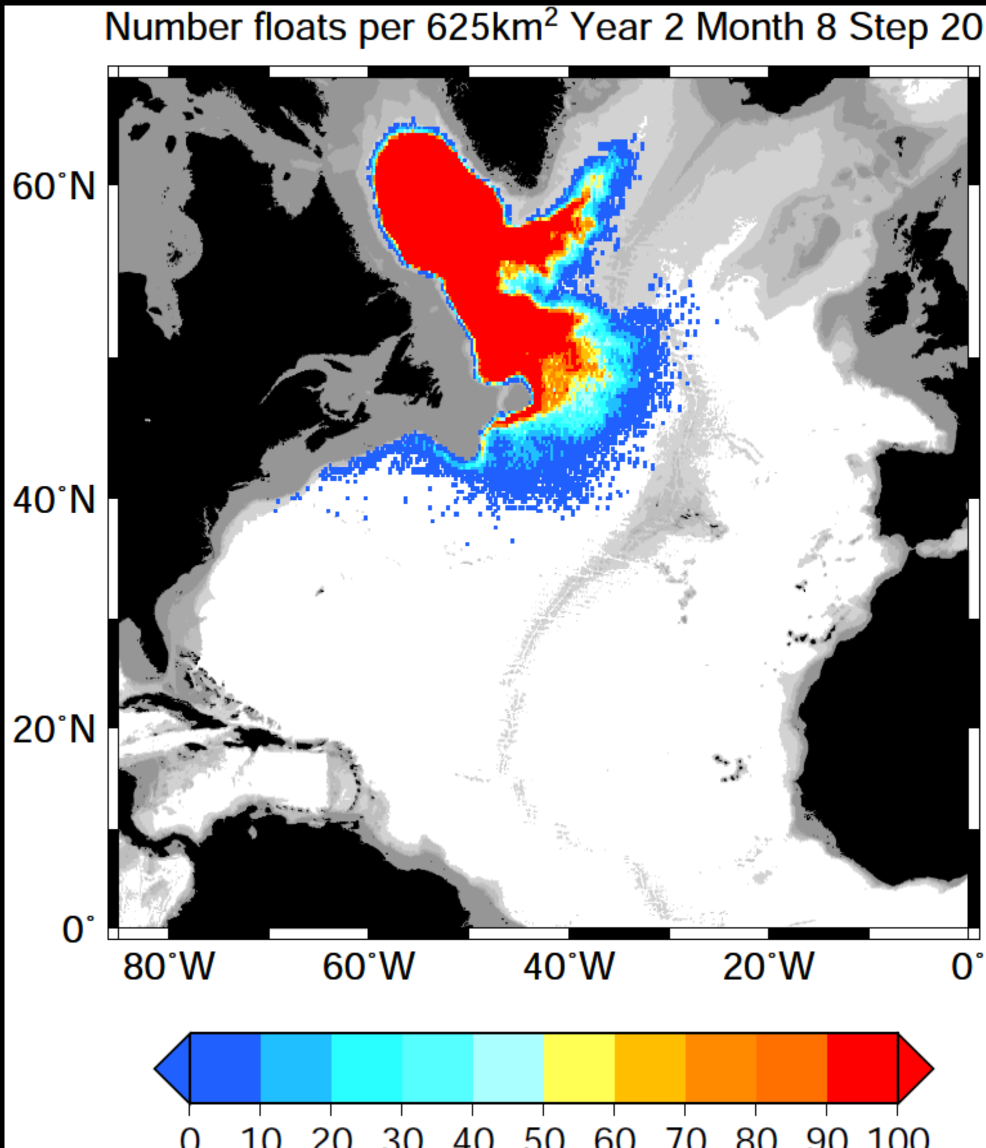

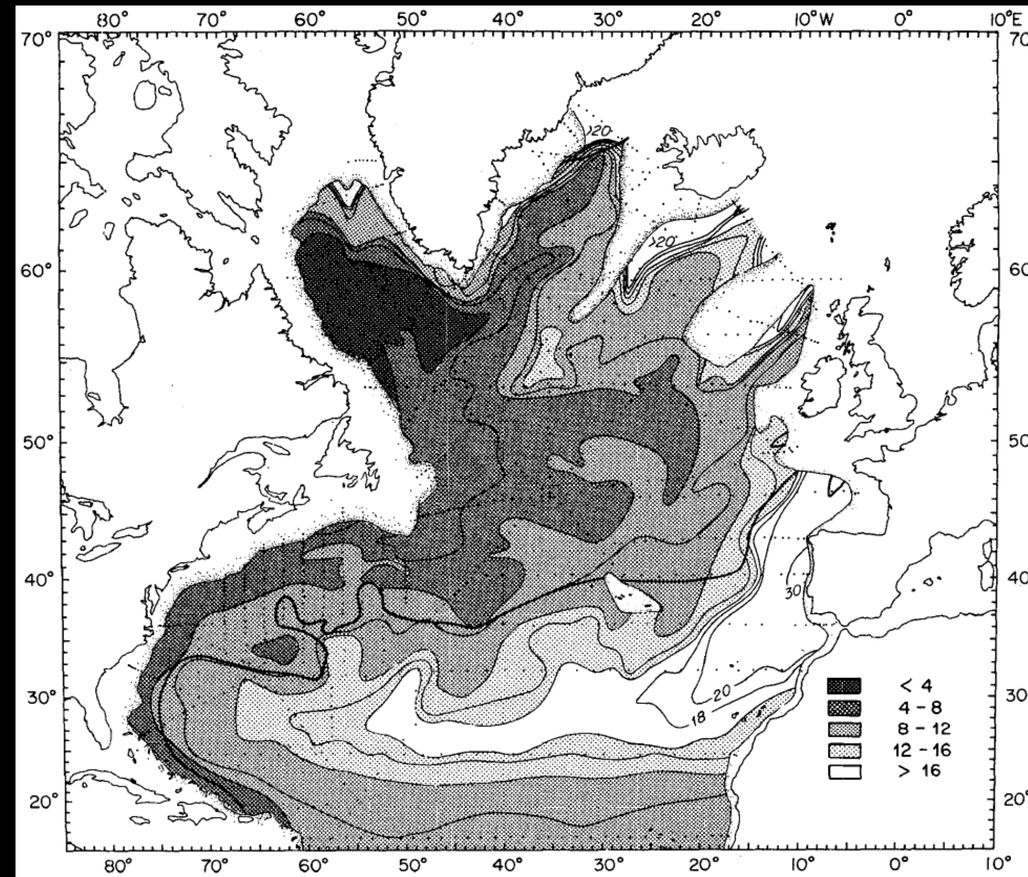

FIG. 3. Potential vorticity $(f/\rho)(\delta\rho/\delta z)$, in units of 10^{-14} cm^{-1} s^{-1}, at the LSW potential vorticity minimum, using the data of Fig. 1 The potential vorticity is a local measure of the vertical homogeneity of the water mass. The heavy curves are the limits of the identifiabl LSW potential vorticity minimum. Beyond these curves, contouring is continued on the σ_{1500} = 34.72 mg cm^{-3} surface. Contou intervals are 2×10^{-14} cm^{-1} s^{-1}.

(Talley & McCartney, 1982)

9.7×10^5 Lagrangian particles launched below 1000m at potential vorticities < 3×10^{-12} m^{-1}s^{-1}. Trajectories were integrated in the repeated, 5-day mean 1990 - 2004 ORCA025 velocity fields for 50 years.

Lagrangian Pathways and Tracer

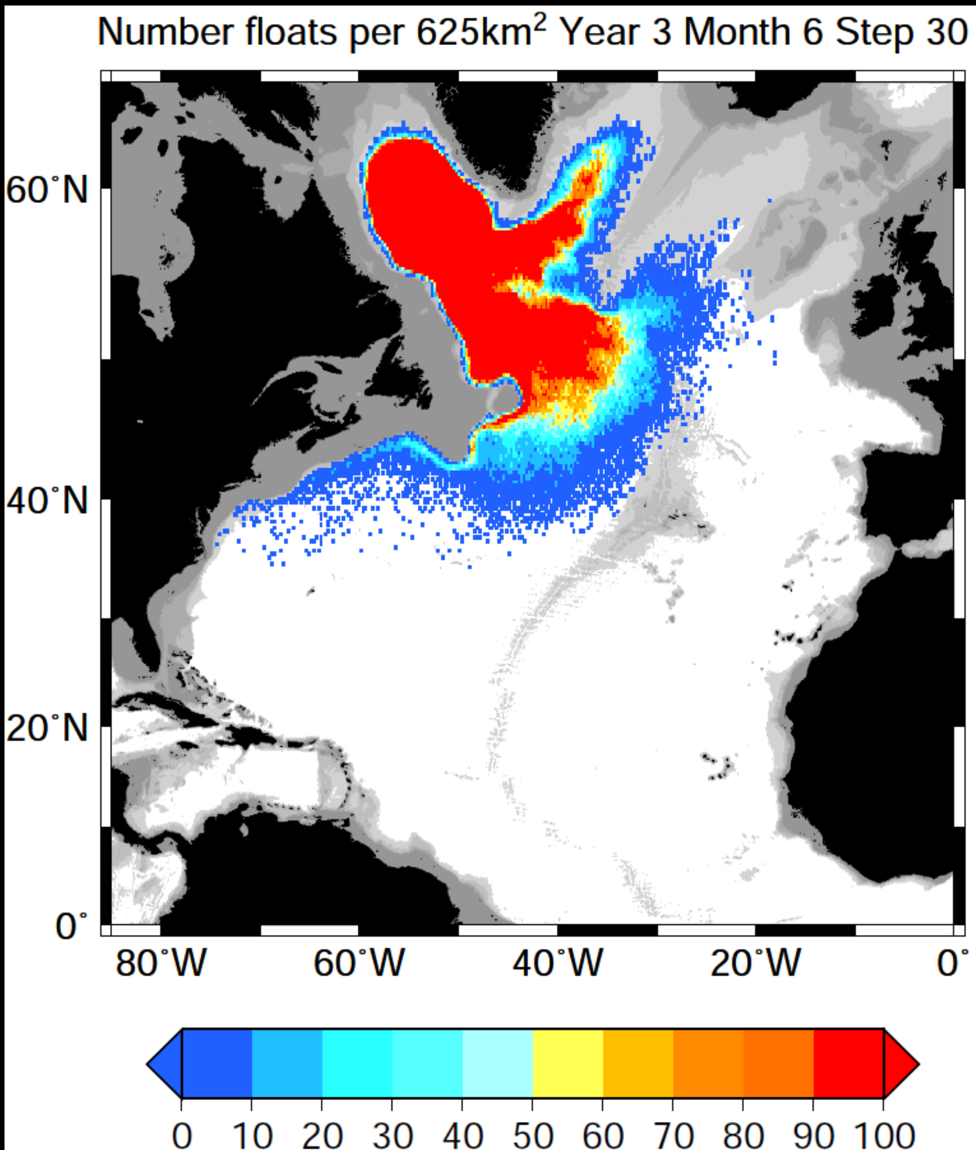

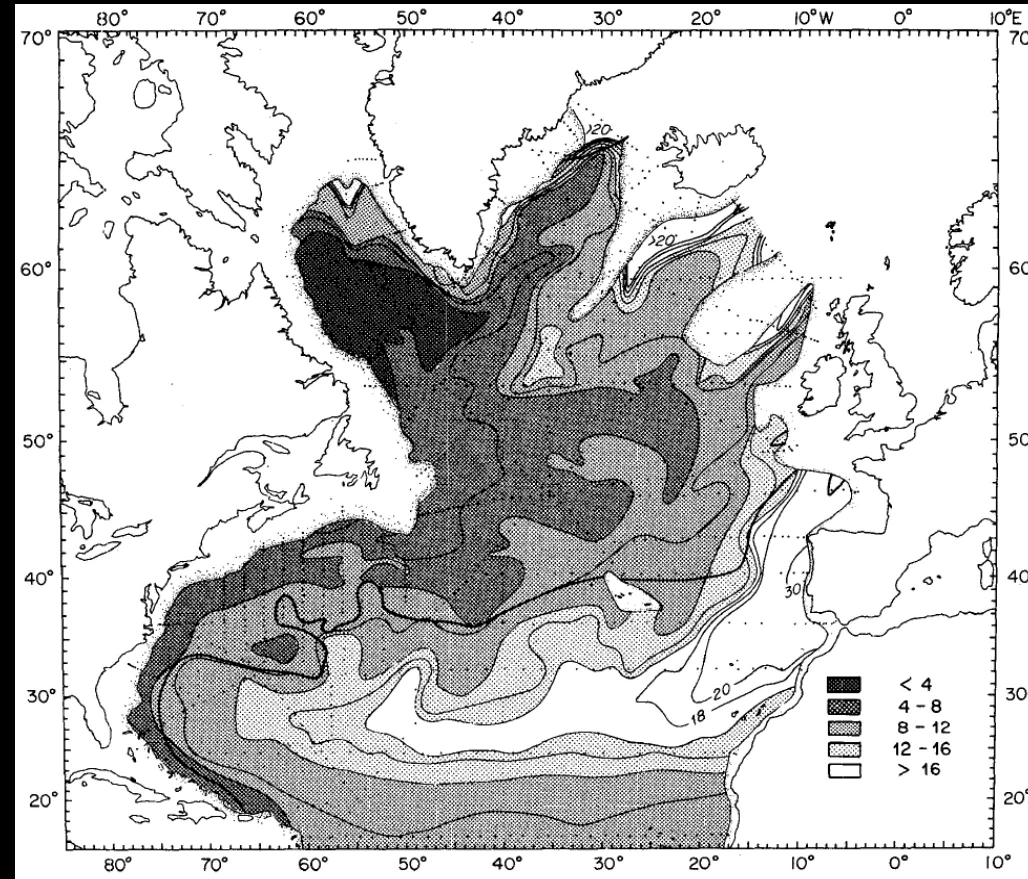

FIG. 3. Potential vorticity $(f/\rho)(\delta\rho/\delta z)$, in units of 10^{-14} cm^{-1} s^{-1}, at the LSW potential vorticity minimum, using the data of Fig. l The potential vorticity is a local measure of the vertical homogeneity of the water mass. The heavy curves are the limits of the identifiabl LSW potential vorticity minimum. Beyond these curves, contouring is continued on the σ_{1500} = 34.72 mg cm^{-3} surface. Contou intervals are 2×10^{-14} cm^{-1} s^{-1}.

(Talley & McCartney, 1982)

9.7×10^5 Lagrangian particles launched below 1000m at potential vorticities < 3×10^{-12} m^{-1}s^{-1}. Trajectories were integrated in the repeated, 5-day mean 1990 - 2004 ORCA025 velocity fields for 50 years.

Lagrangian Pathways and Tracer

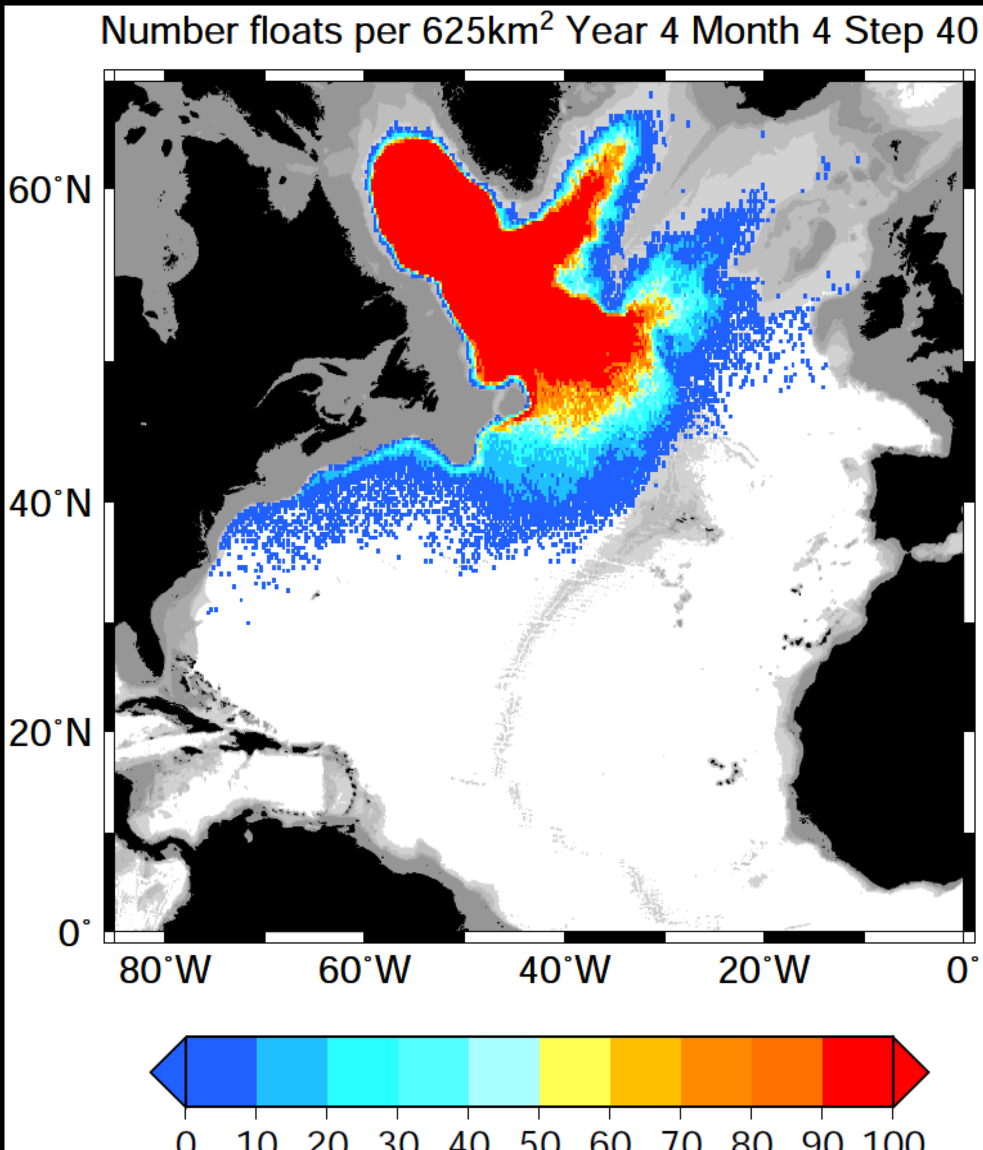

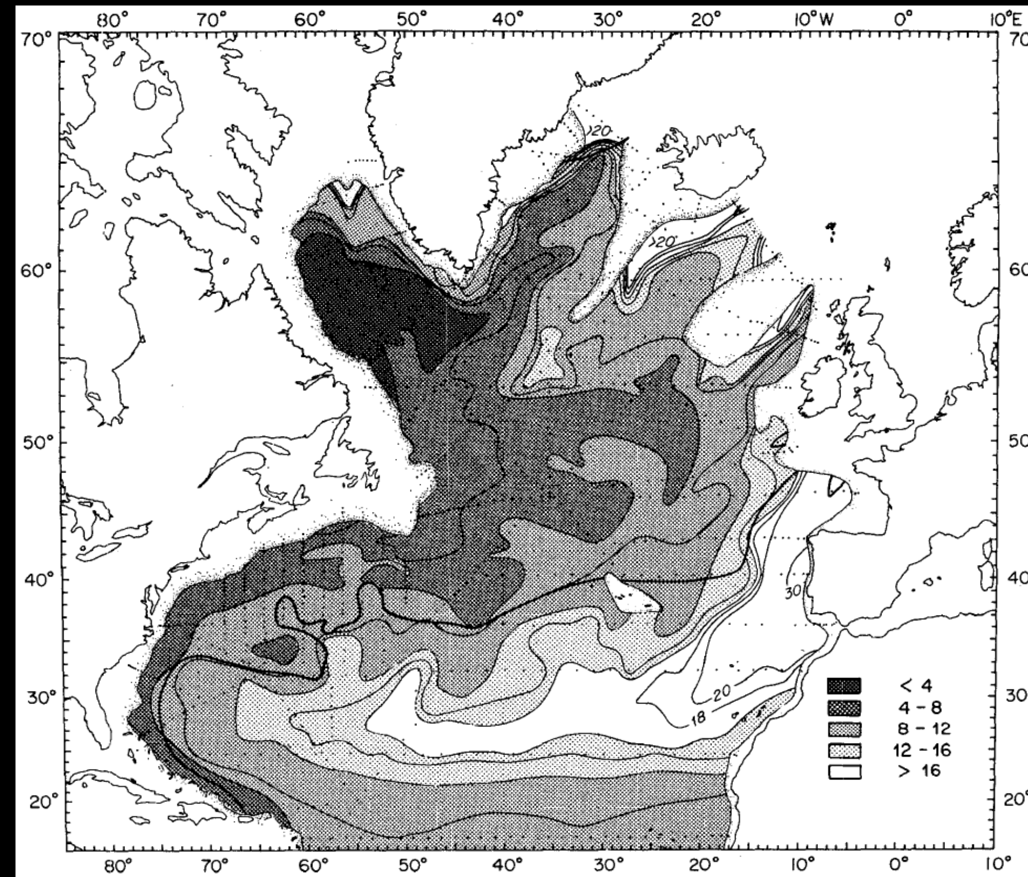

FIG. 3. Potential vorticity $(f/\rho)(\delta\rho/\delta z)$, in units of 10^{-14} cm^{-1} s^{-1}, at the LSW potential vorticity minimum, using the data of Fig. 1 The potential vorticity is a local measure of the vertical homogeneity of the water mass. The heavy curves are the limits of the identifiabl LSW potential vorticity minimum. Beyond these curves, contouring is continued on the σ_{1500} = 34.72 mg cm^{-3} surface. Contou intervals are 2×10^{-14} cm^{-1} s^{-1}.

(Talley & McCartney, 1982)

9.7×10^{5} Lagrangian particles launched below 1000m at potential vorticities < 3×10^{-12} m^{-1}s^{-1}. Trajectories were integrated in the repeated, 5-day mean 1990 - 2004 ORCA025 velocity fields for 50 years.

Lagrangian Pathways and Tracer

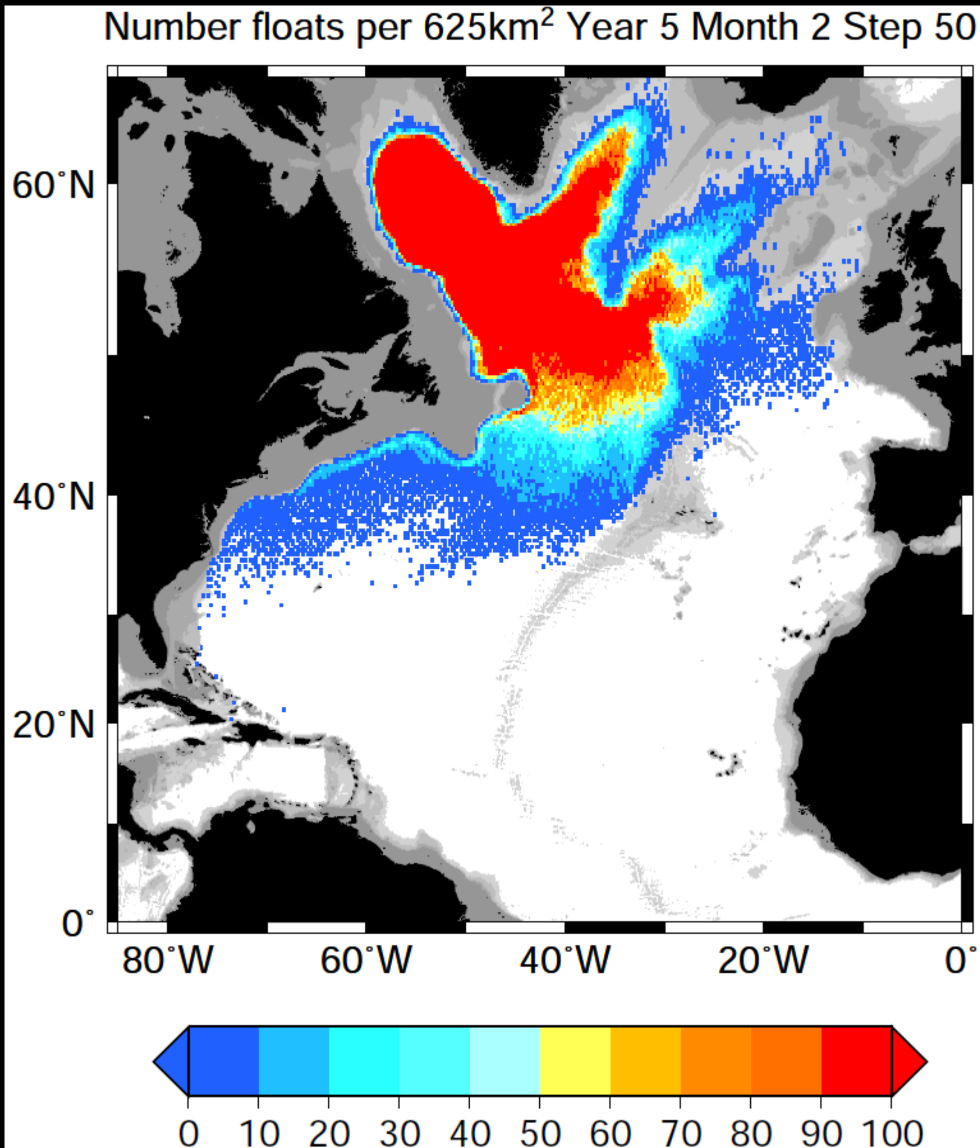

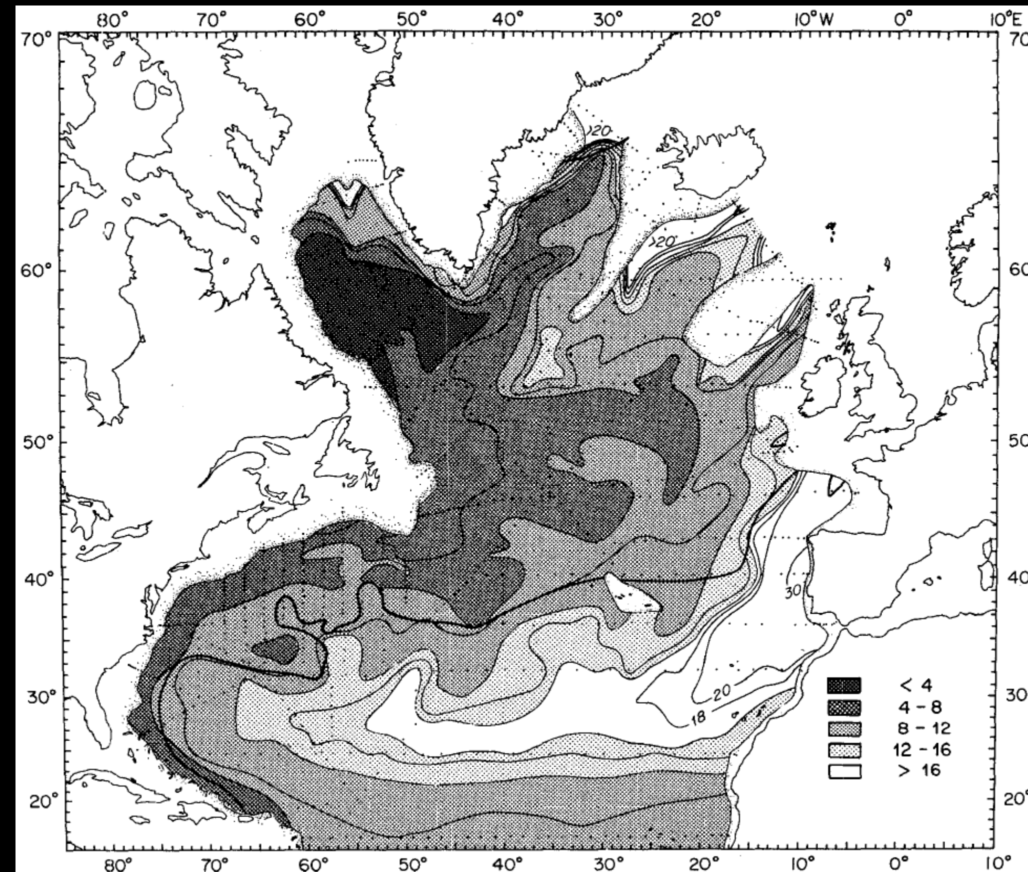

FIG. 3. Potential vorticity $(f/\rho)(\delta\rho/\delta z)$, in units of 10^{-14} cm^{-1} s^{-1}, at the LSW potential vorticity minimum, using the data of Fig. 1 The potential vorticity is a local measure of the vertical homogeneity of the water mass. The heavy curves are the limits of the identifiabl LSW potential vorticity minimum. Beyond these curves, contouring is continued on the σ_{1500} = 34.72 mg cm^{-3} surface. Contou intervals are 2×10^{-14} cm^{-1} s^{-1}.

(Talley & McCartney, 1982)

9.7×10^5 Lagrangian particles launched below 1000m at potential vorticities < 3×10^{-12} m^{-1}s^{-1}. Trajectories were integrated in the repeated, 5-day mean 1990 - 2004 ORCA025 velocity fields for 50 years.

Lagrangian Pathways and Tracer

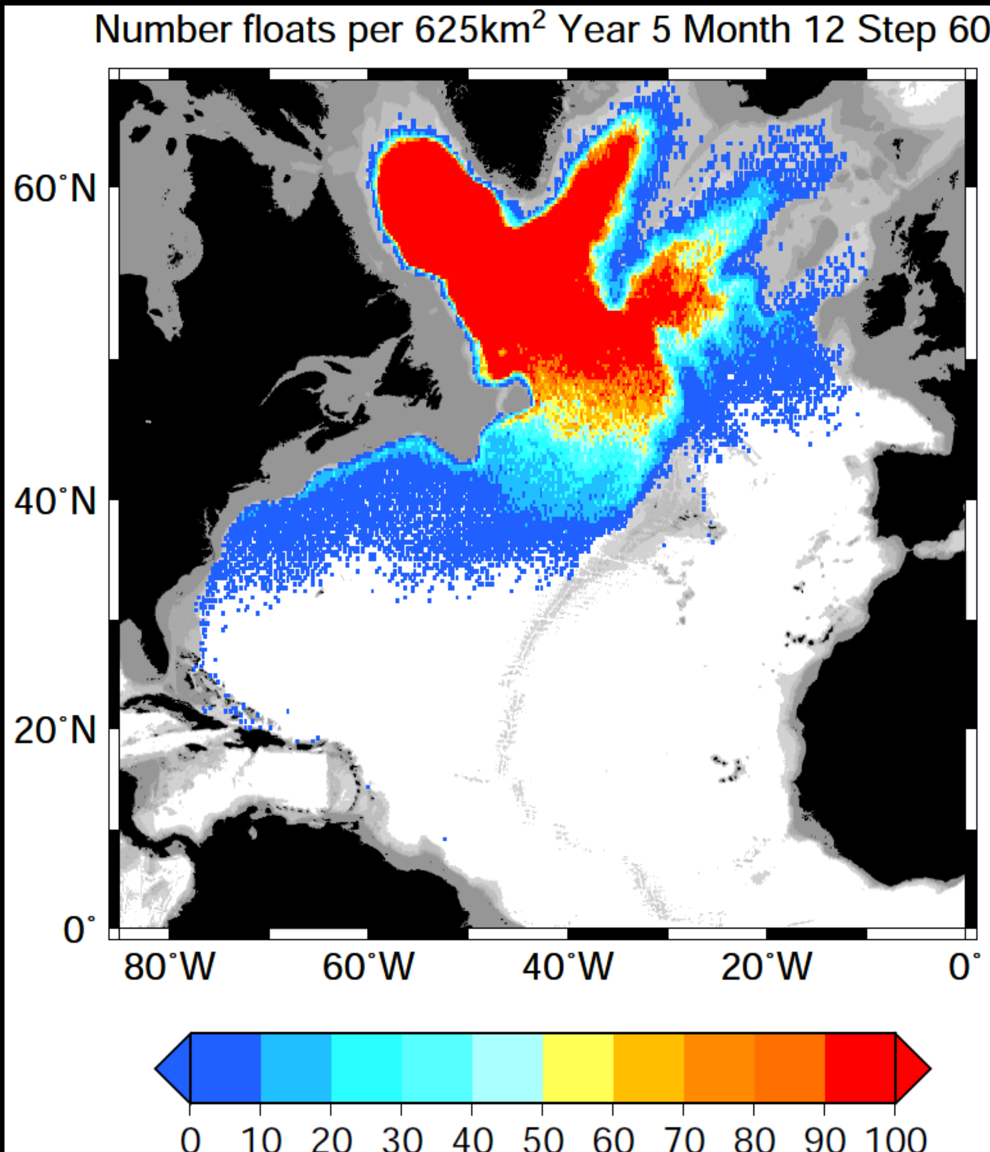

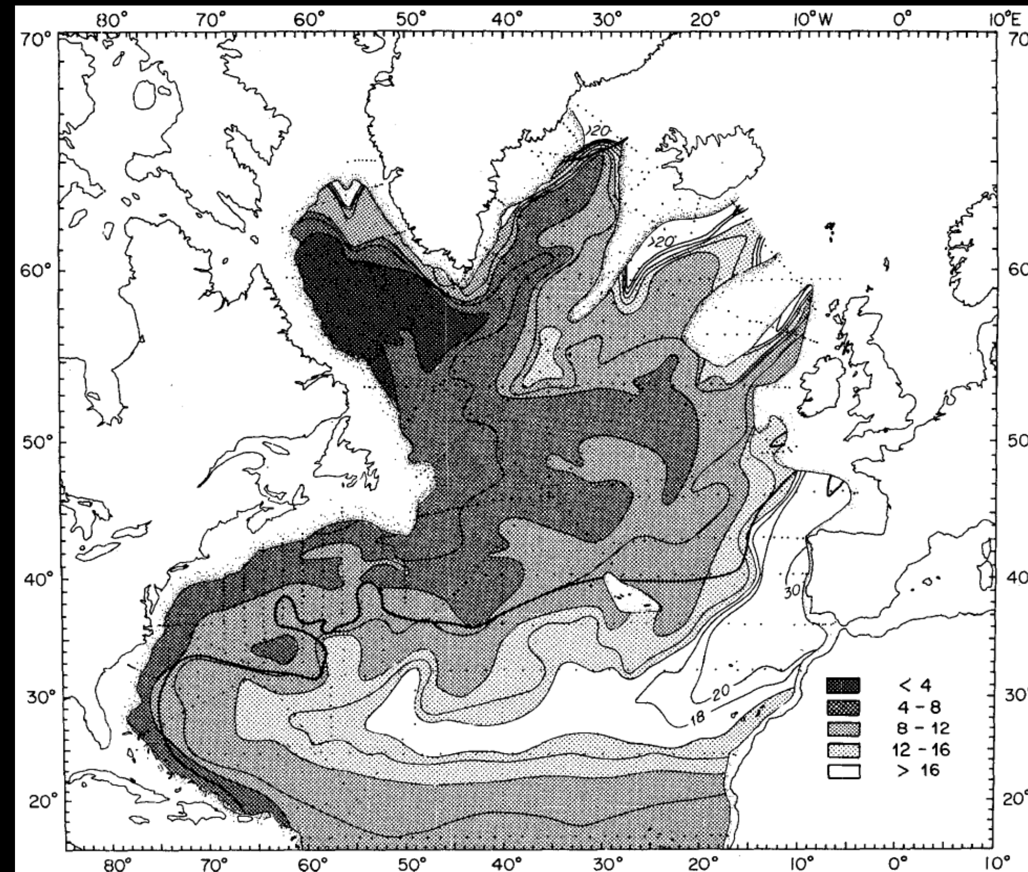

FIG. 3. Potential vorticity $(f/\rho)(\delta\rho/\delta z)$, in units of 10^{-14} cm^{-1} s^{-1}, at the LSW potential vorticity minimum, using the data of Fig. 1 The potential vorticity is a local measure of the vertical homogeneity of the water mass. The heavy curves are the limits of the identifiabl LSW potential vorticity minimum. Beyond these curves, contouring is continued on the σ_{1500} = 34.72 mg cm^{-3} surface. Contou intervals are 2×10^{-14} cm^{-1} s^{-1}.

(Talley & McCartney, 1982)

9.7×10^5 Lagrangian particles launched below 1000m at potential vorticities < 3×10^{-12} m^{-1}s^{-1}. Trajectories were integrated in the repeated, 5-day mean 1990 - 2004 ORCA025 velocity fields for 50 years.

Lagrangian Pathways and Tracer

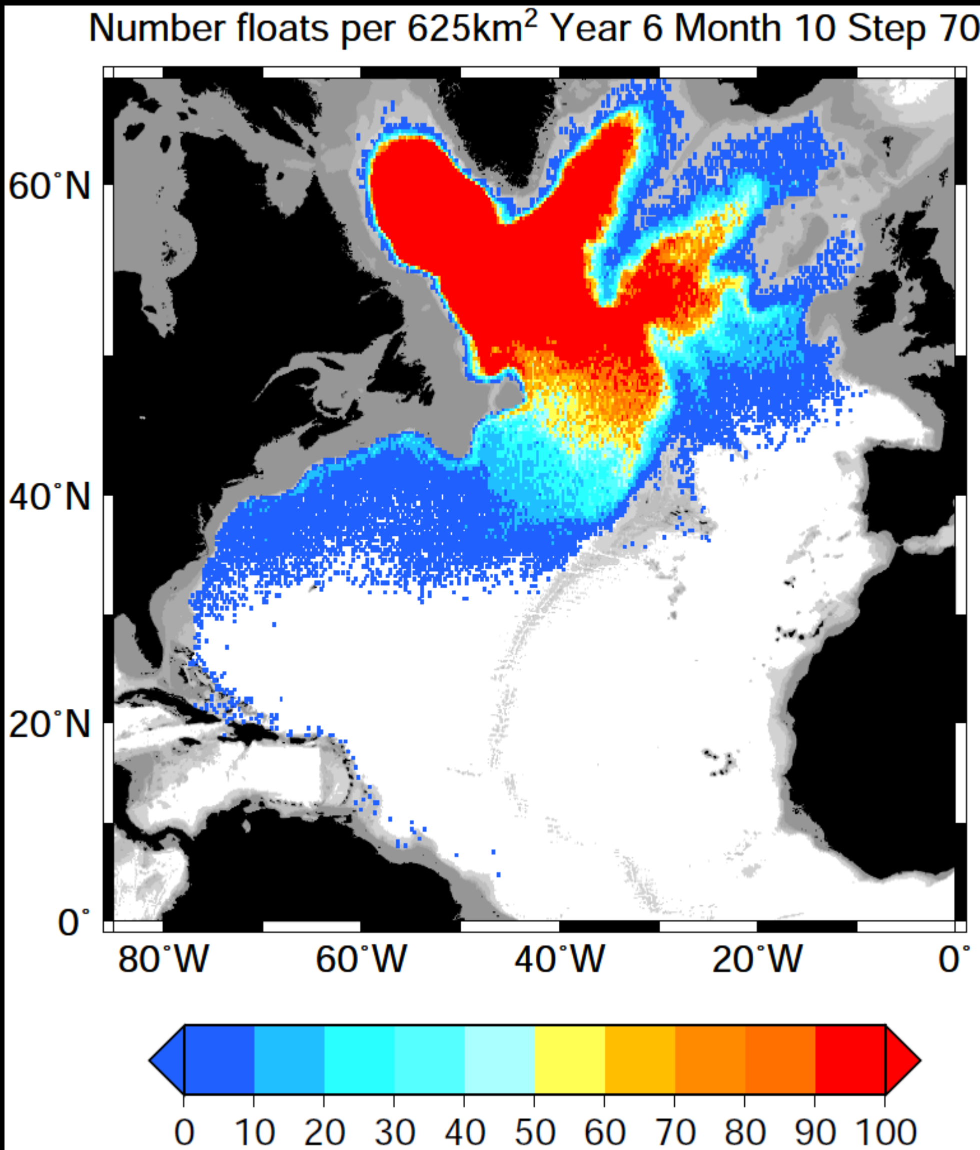

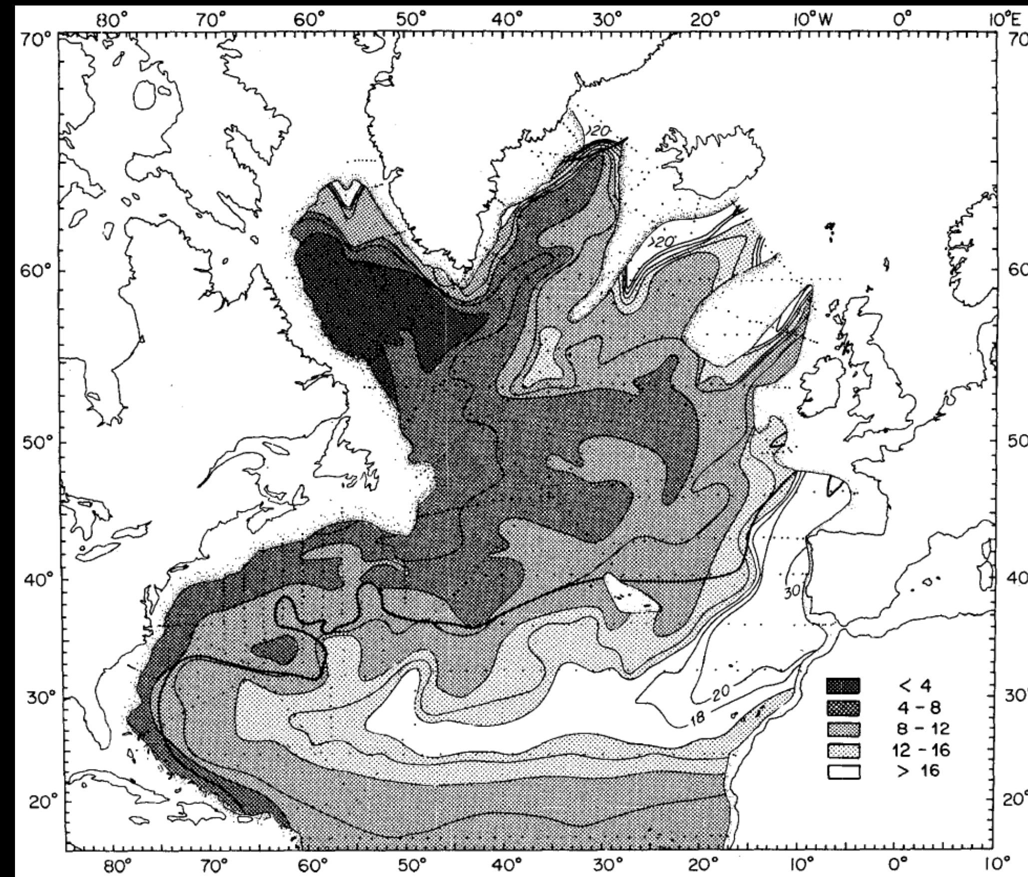

FIG. 3. Potential vorticity $(f/\rho)(\delta\rho/\delta z)$, in units of 10^{-14} cm^{-1} s^{-1}, at the LSW potential vorticity minimum, using the data of Fig. 1 The potential vorticity is a local measure of the vertical homogeneity of the water mass. The heavy curves are the limits of the identifiable LSW potential vorticity minimum. Beyond these curves, contouring is continued on the σ_{1500} = 34.72 mg cm^{-3} surface. Contour intervals are 2×10^{-14} cm^{-1} s^{-1}.

(Talley & McCartney, 1982)

9.7×10^5 Lagrangian particles launched below 1000m at potential vorticities < 3×10^{-12} m^{-1}s^{-1}. Trajectories were integrated in the repeated, 5-day mean 1990 - 2004 ORCA025 velocity fields for 50 years.

Lagrangian Pathways and Tracer

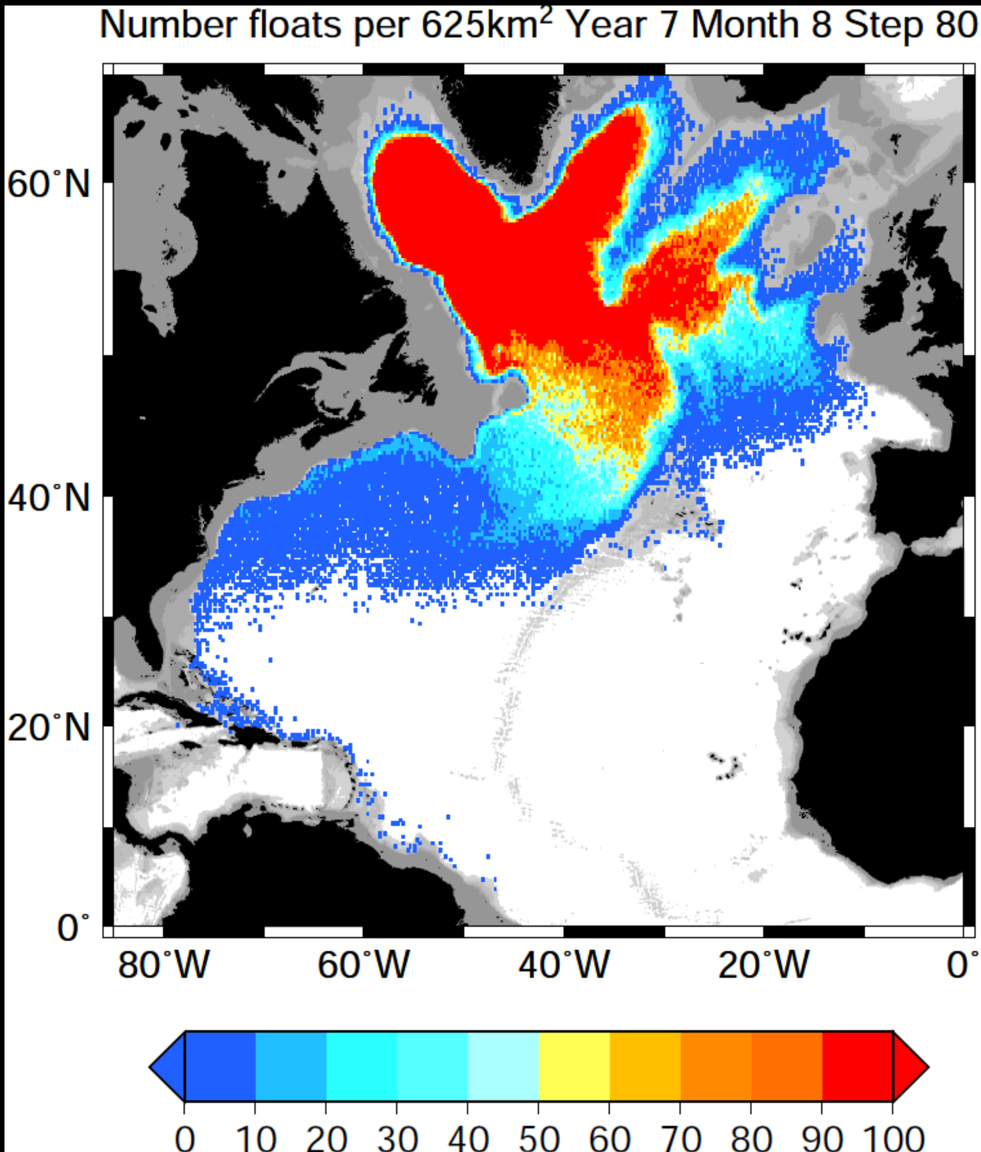

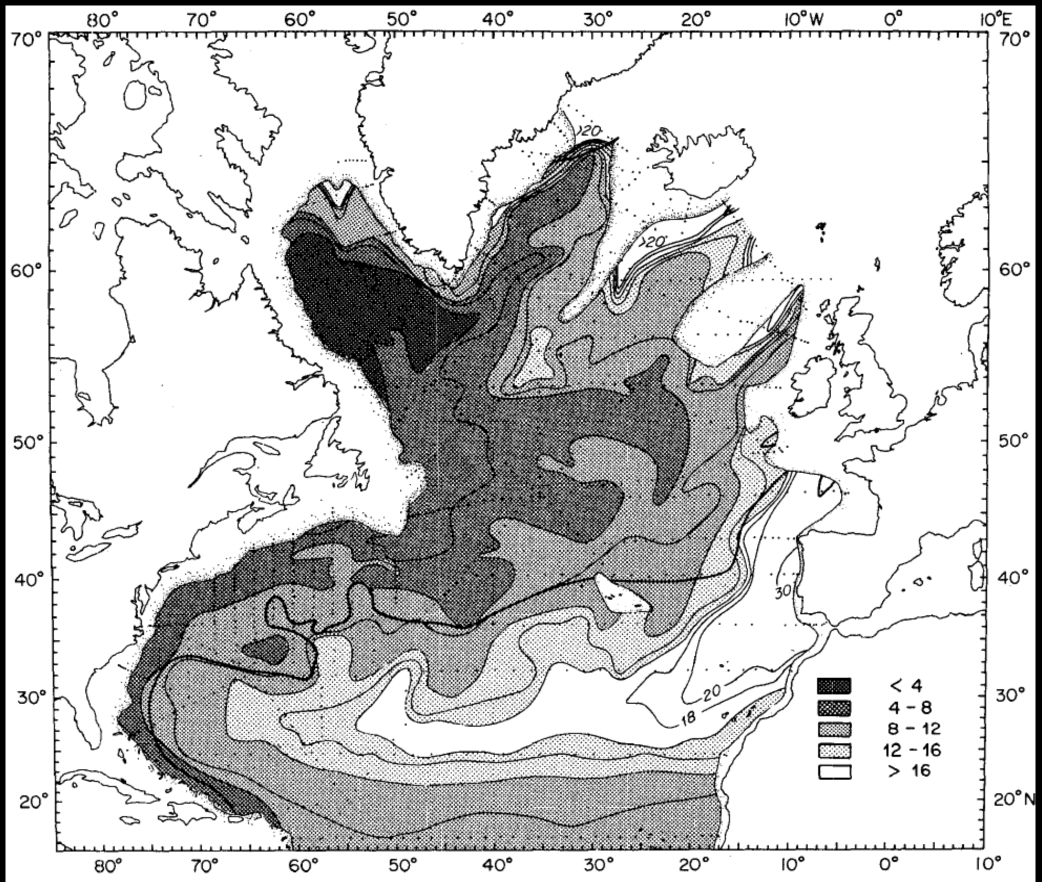

FIG. 3. Potential vorticity $(f/\rho)(\delta\rho/\delta z)$, in units of 10^{-14} cm^{-1} s^{-1}, at the LSW potential vorticity minimum, using the data of Fig. 1 The potential vorticity is a local measure of the vertical homogeneity of the water mass. The heavy curves are the limits of the identifiabl LSW potential vorticity minimum. Beyond these curves, contouring is continued on the σ_{1500} = 34.72 mg cm^{-3} surface. Contou intervals are 2×10^{-14} cm^{-1} s^{-1}.

(Talley & McCartney, 1982)

9.7×10^5 Lagrangian particles launched below 1000m at potential vorticities < 3×10^{-12} m^{-1}s^{-1}. Trajectories were integrated in the repeated, 5-day mean 1990 - 2004 ORCA025 velocity fields for 50 years.

Lagrangian Pathways and Tracer

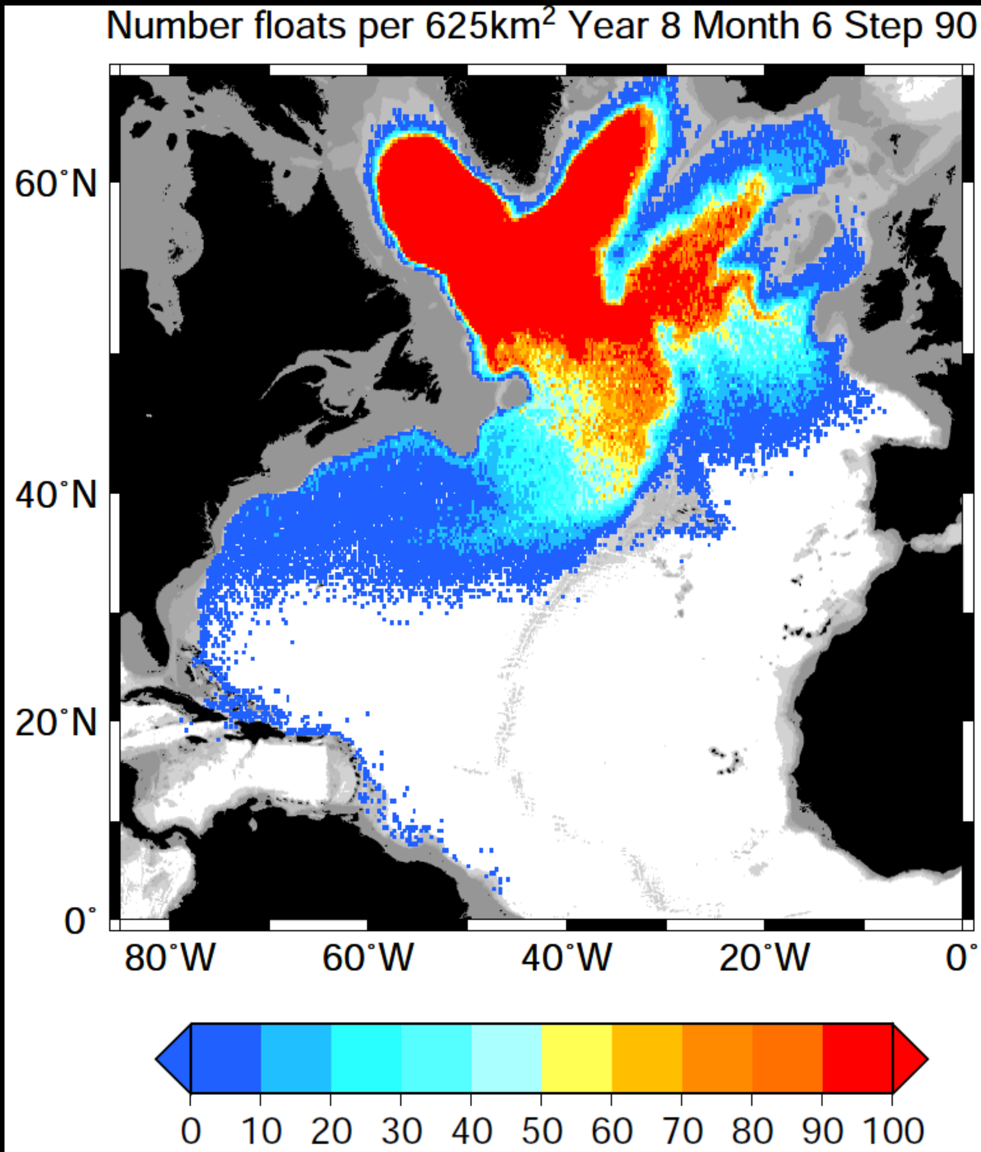

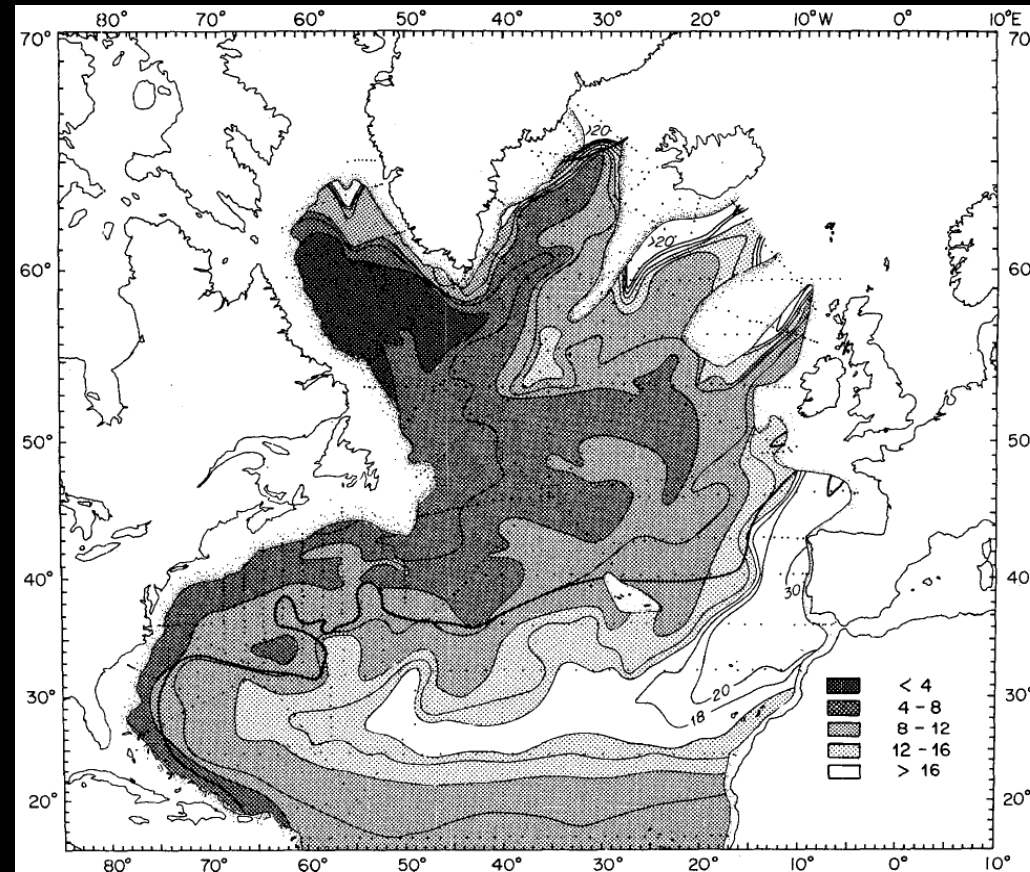

FIG. 3. Potential vorticity $(f/\rho)(\delta\rho/\delta z)$, in units of 10^{-14} cm^{-1} s^{-1}, at the LSW potential vorticity minimum, using the data of Fig. 1. The potential vorticity is a local measure of the vertical homogeneity of the water mass. The heavy curves are the limits of the identifiable LSW potential vorticity minimum. Beyond these curves, contouring is continued on the σ_{1500} = 34.72 mg cm^{-3} surface. Contour intervals are 2×10^{-14} cm^{-1} s^{-1}.

(Talley & McCartney, 1982)

9.7×10^5 Lagrangian particles launched below 1000m at potential vorticities < 3×10^{-12} $m^{-1}s^{-1}$. Trajectories were integrated in the repeated, 5-day mean 1990 - 2004 ORCA025 velocity fields for 50 years.

Lagrangian Pathways and Tracer

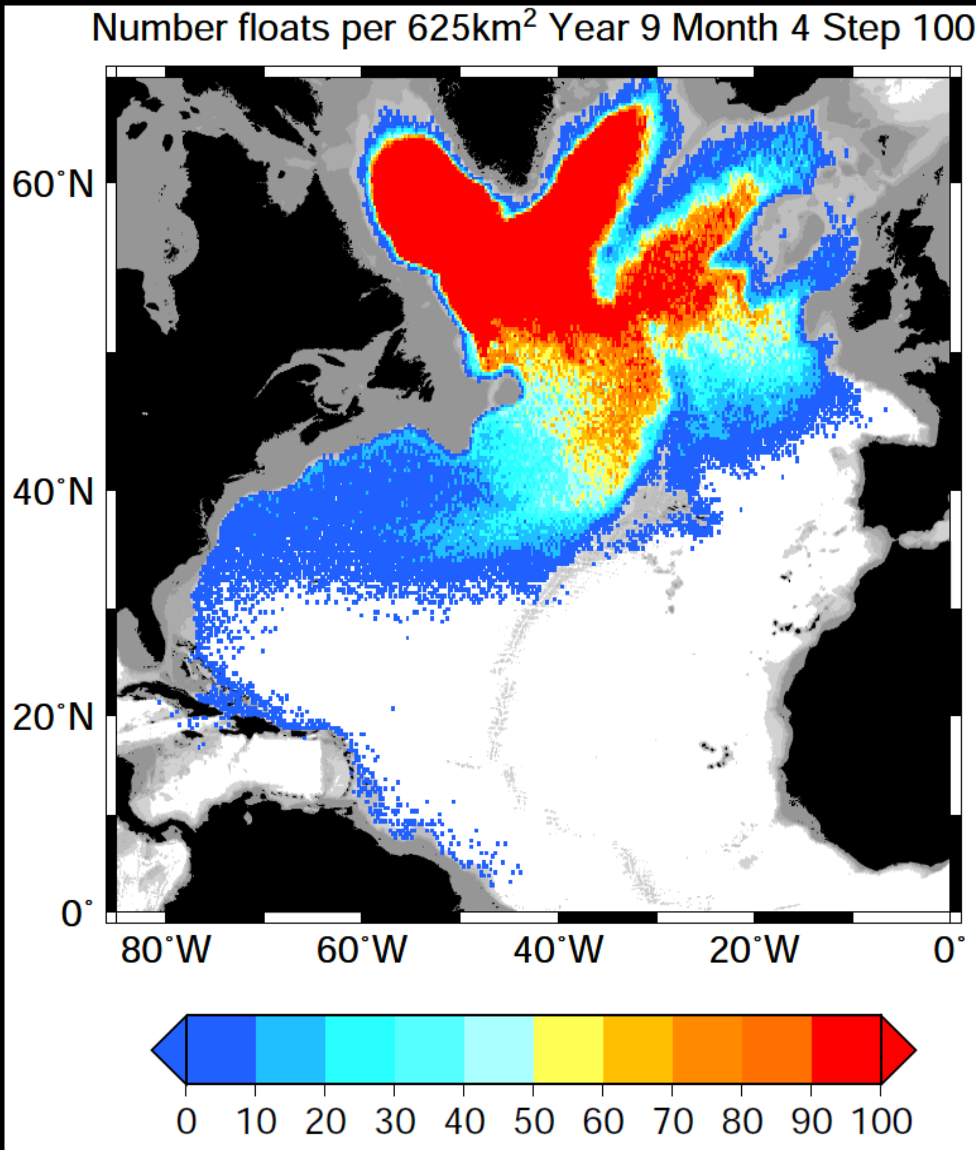

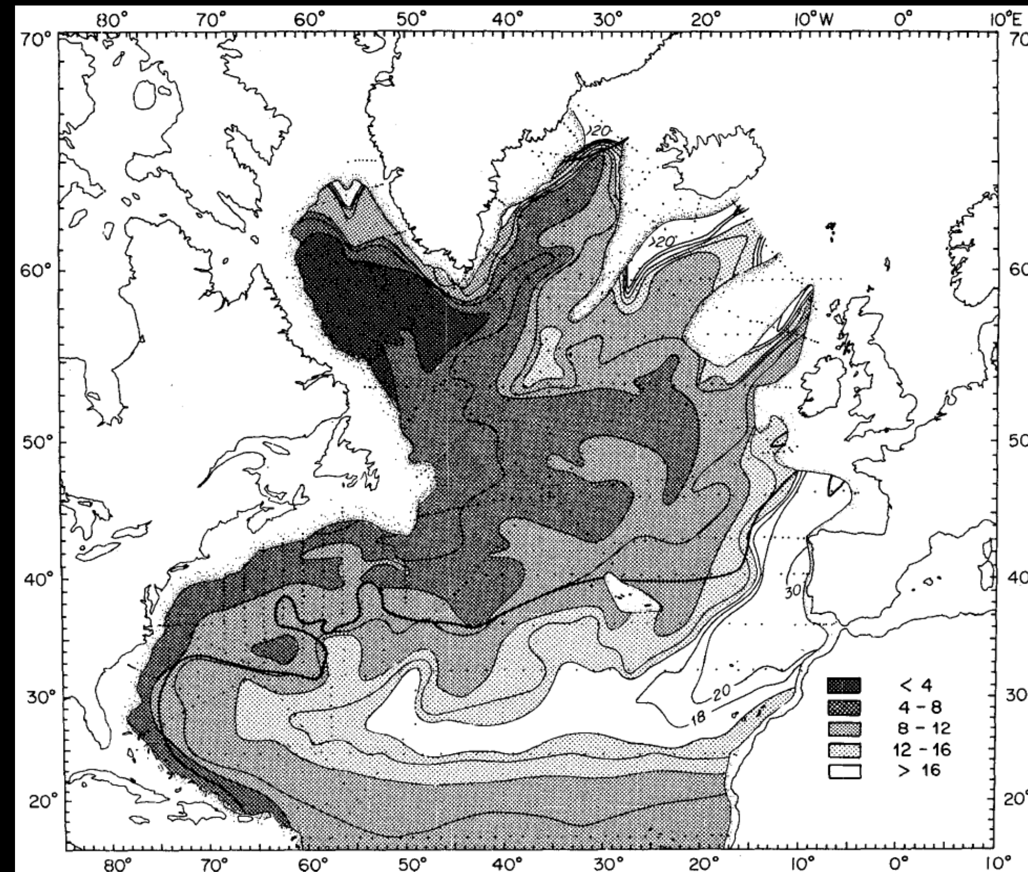

FIG. 3. Potential vorticity $(f/\rho)(\delta\rho/\delta z)$, in units of 10^{-14} cm^{-1} s^{-1}, at the LSW potential vorticity minimum, using the data of Fig. 1 The potential vorticity is a local measure of the vertical homogeneity of the water mass. The heavy curves are the limits of the identifiabl LSW potential vorticity minimum. Beyond these curves, contouring is continued on the σ_{1500} = 34.72 mg cm^{-3} surface. Contou intervals are 2×10^{-14} cm^{-1} s^{-1}.

(Talley & McCartney, 1982)

9.7×10^5 Lagrangian particles launched below 1000m at potential vorticities < 3×10^{-12} $m^{-1}s^{-1}$. Trajectories were integrated in the repeated, 5-day mean 1990 - 2004 ORCA025 velocity fields for 50 years.

Lagrangian Pathways and Tracer

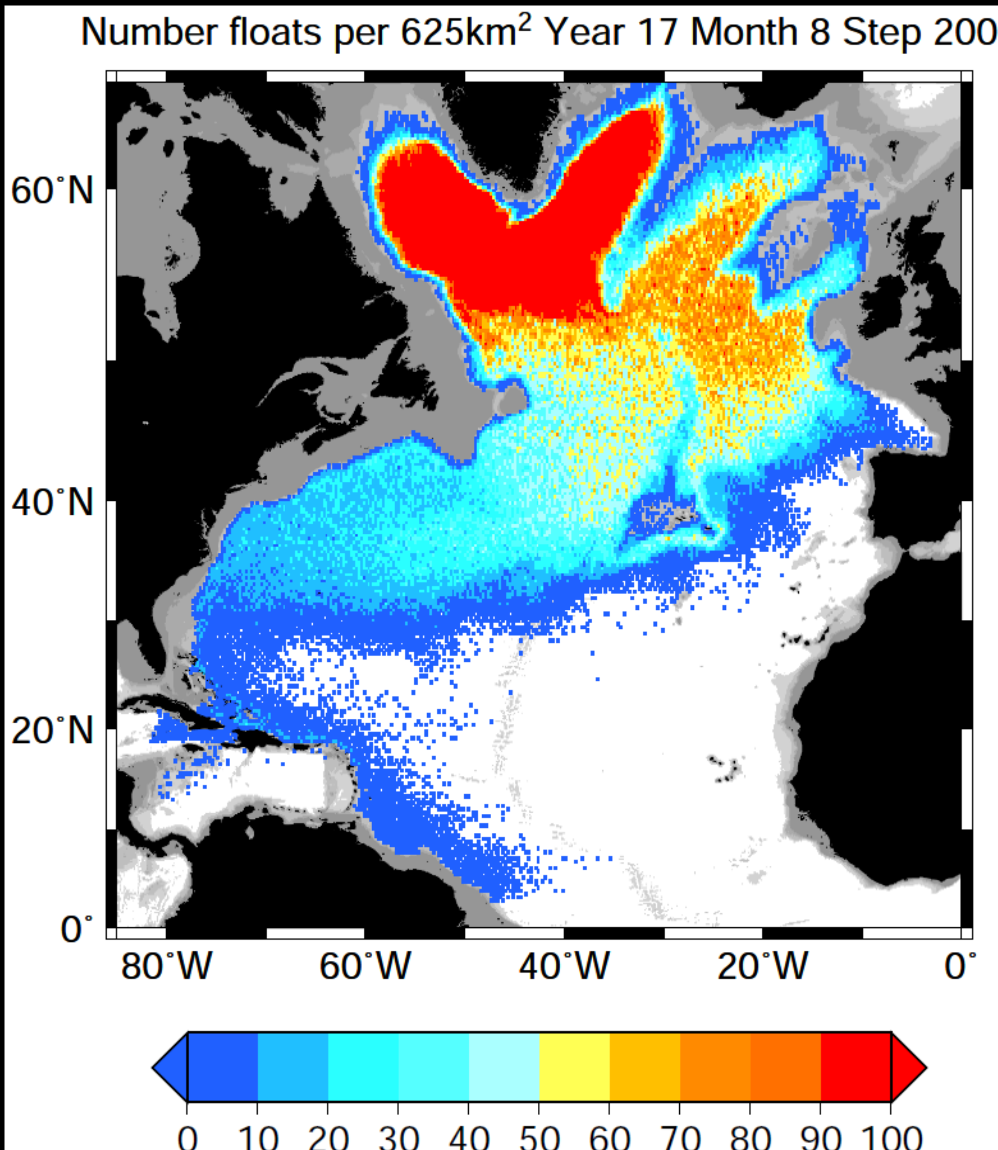

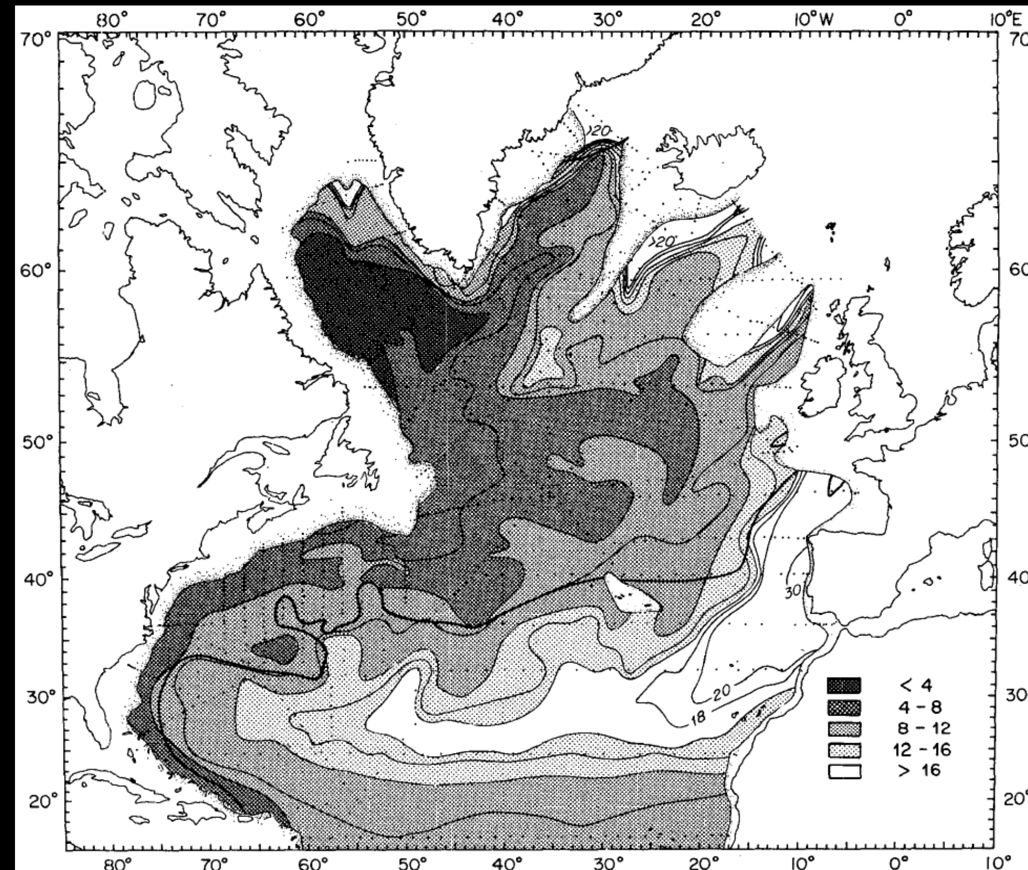

FIG. 3. Potential vorticity $(f/\rho)(\delta\rho/\delta z)$, in units of 10^{-14} cm^{-1} s^{-1}, at the LSW potential vorticity minimum, using the data of Fig. 1 The potential vorticity is a local measure of the vertical homogeneity of the water mass. The heavy curves are the limits of the identifiabl LSW potential vorticity minimum. Beyond these curves, contouring is continued on the σ_{1500} = 34.72 mg cm^{-3} surface. Contou intervals are 2×10^{-14} cm^{-1} s^{-1}.

(Talley & McCartney, 1982)

9.7×10^{5} Lagrangian particles launched below 1000m at potential vorticities < 3×10^{-12} m^{-1}s^{-1}. Trajectories were integrated in the repeated, 5-day mean 1990 - 2004 ORCA025 velocity fields for 50 years.

Lagrangian Pathways and Tracer

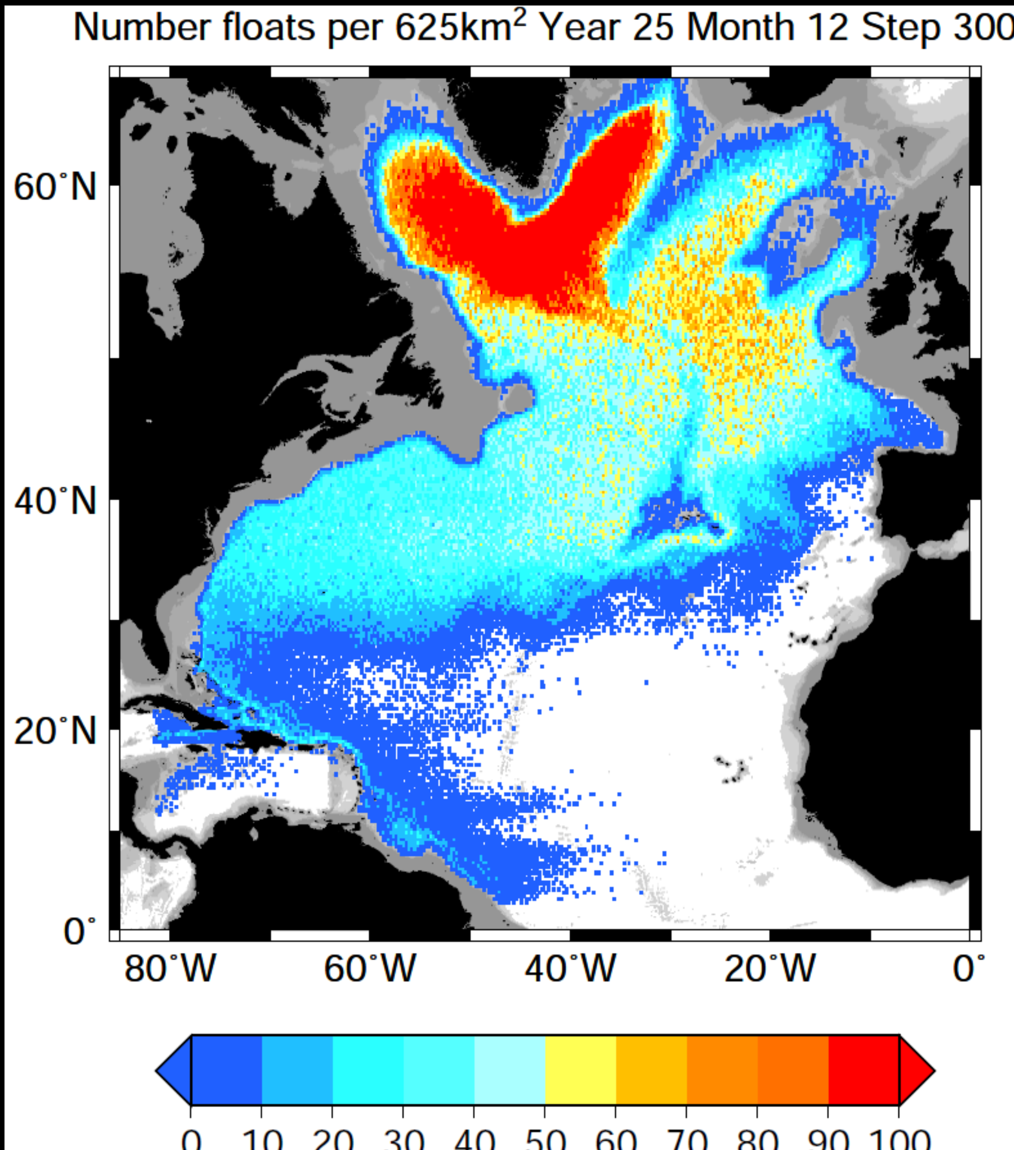

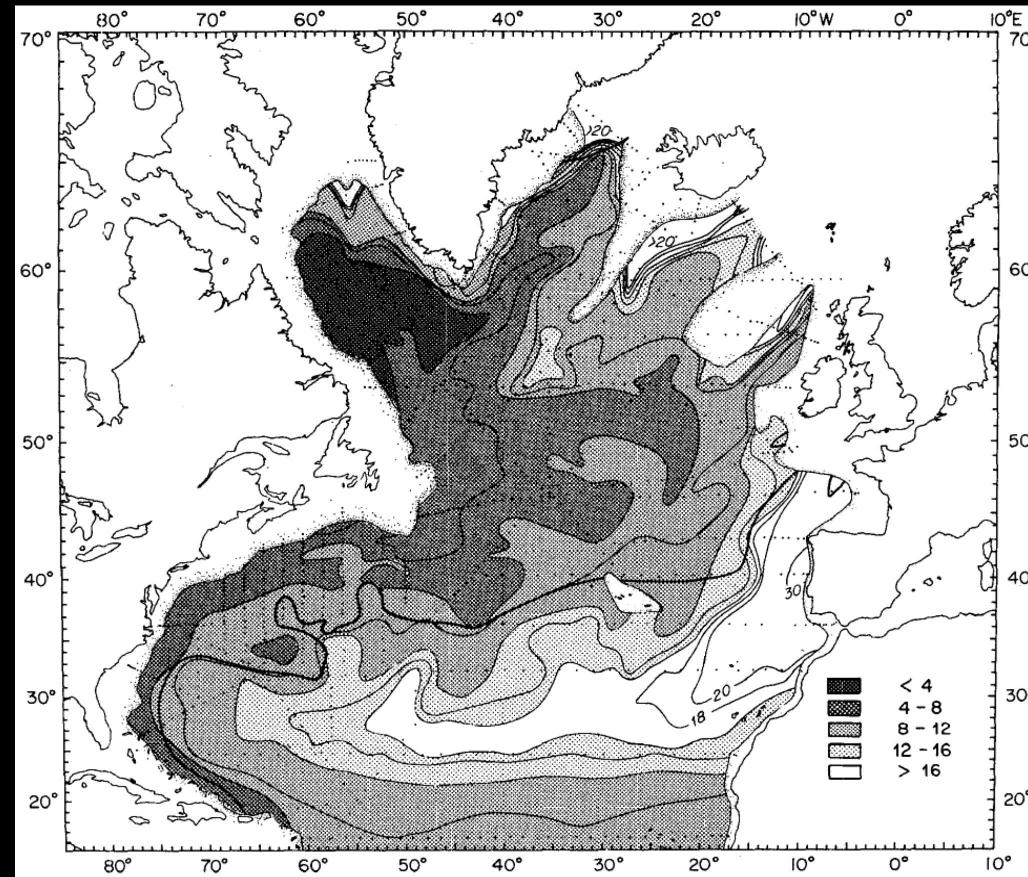

FIG. 3. Potential vorticity $(f/\rho)(\delta\rho/\delta z)$, in units of 10^{-14} cm^{-1} s^{-1}, at the LSW potential vorticity minimum, using the data of Fig. 1. The potential vorticity is a local measure of the vertical homogeneity of the water mass. The heavy curves are the limits of the identifiable LSW potential vorticity minimum. Beyond these curves, contouring is continued on the σ_{1500} = 34.72 mg cm^{-3} surface. Contour intervals are 2×10^{-14} cm^{-1} s^{-1}.

(Talley & McCartney, 1982)

9.7×10^5 Lagrangian particles launched below 1000m at potential vorticities < 3×10^{-12} m^{-1}s^{-1}. Trajectories were integrated in the repeated, 5-day mean 1990 - 2004 ORCA025 velocity fields for 50 years.

Probability distribution

Probability of Lagrangian particle in each ¼° x ¼° grid box over 50 year simulation.

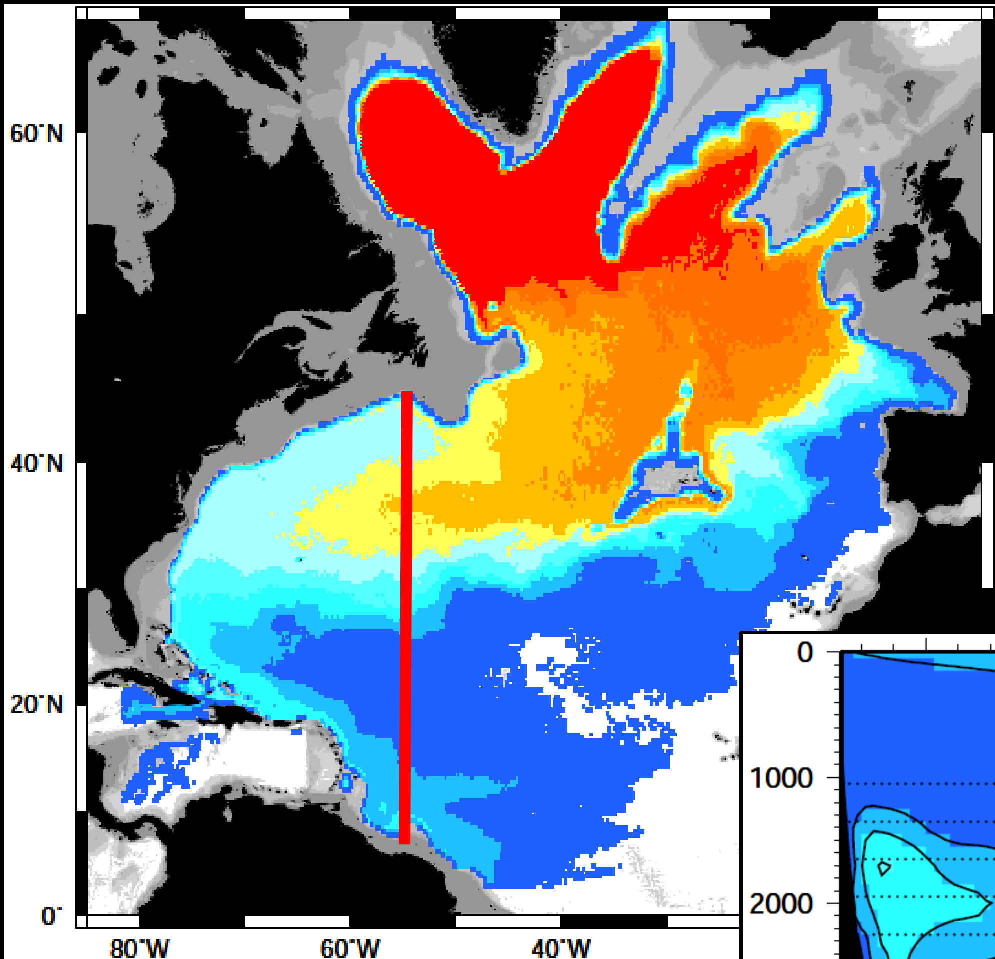

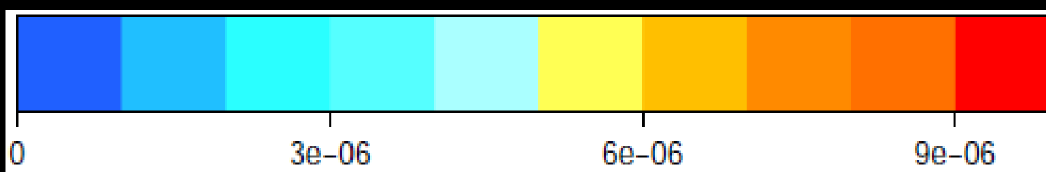

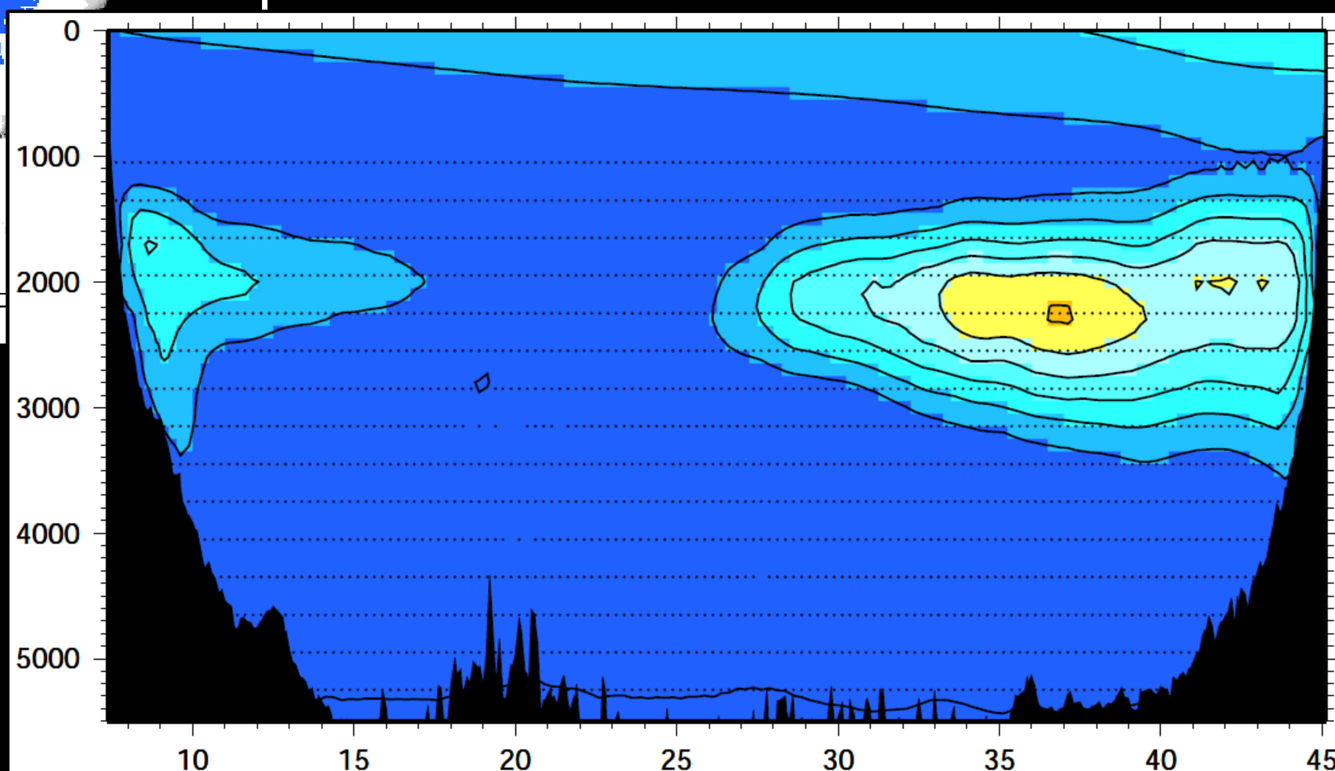

Age distribution

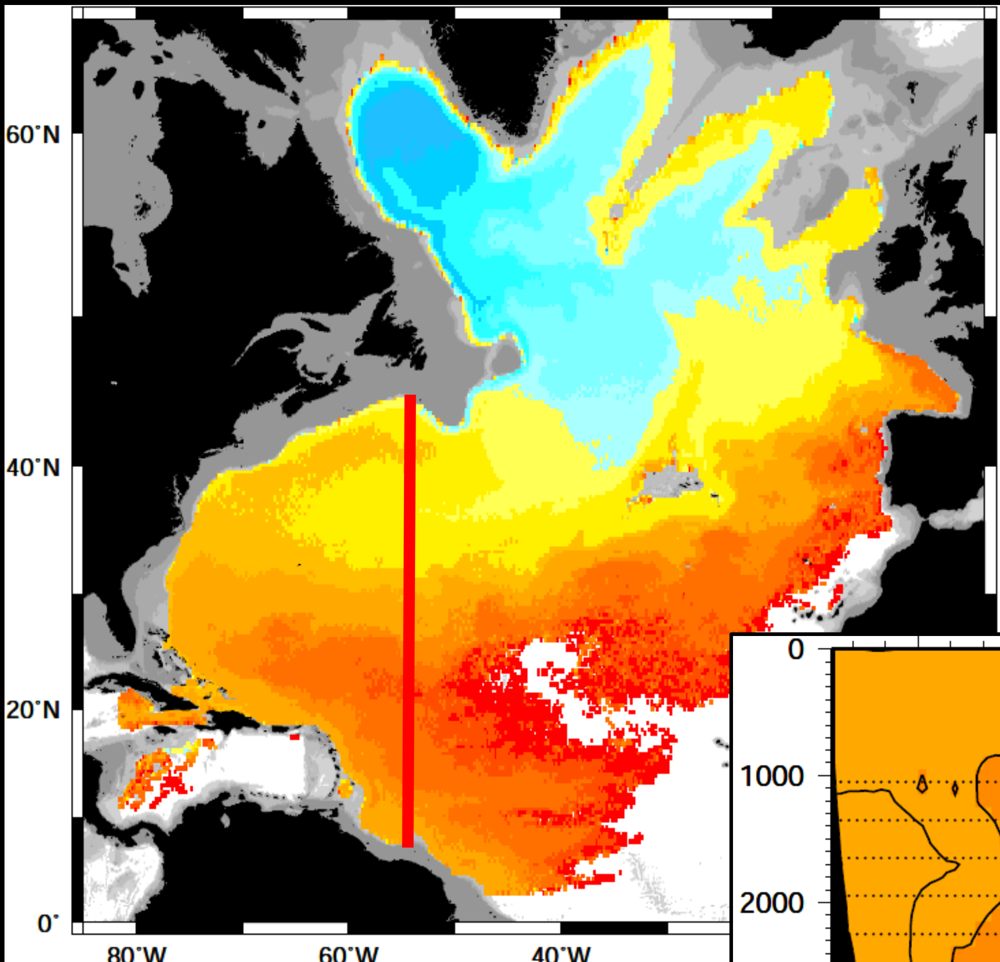

Average age of Lagrangian particles in each ¼° x ¼° grid box over 50 year simulation [years]

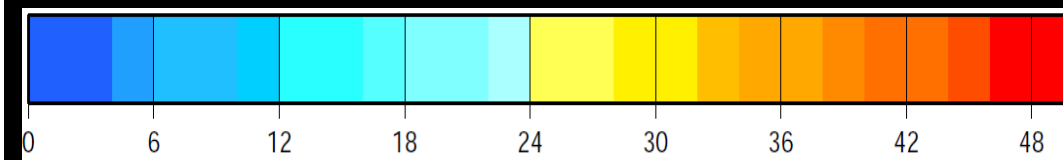

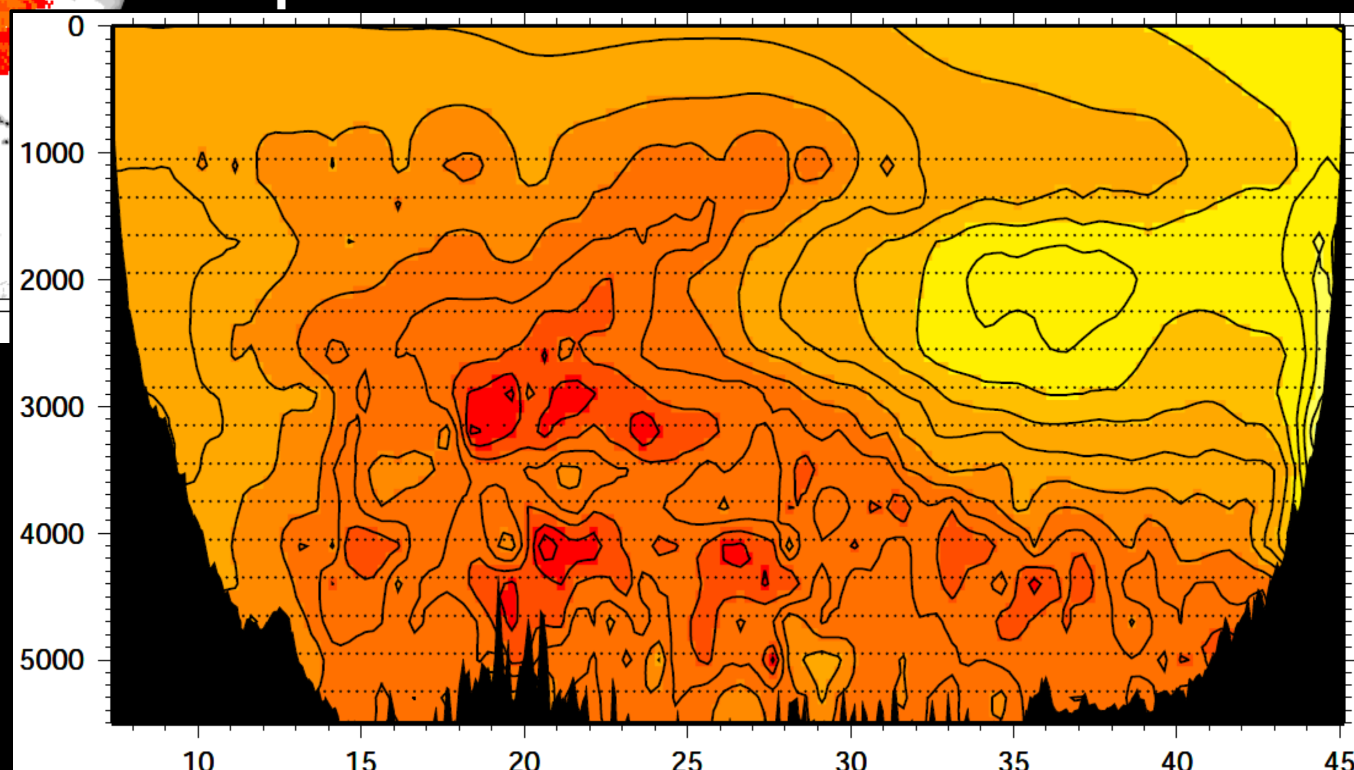

Variability in the age distribution

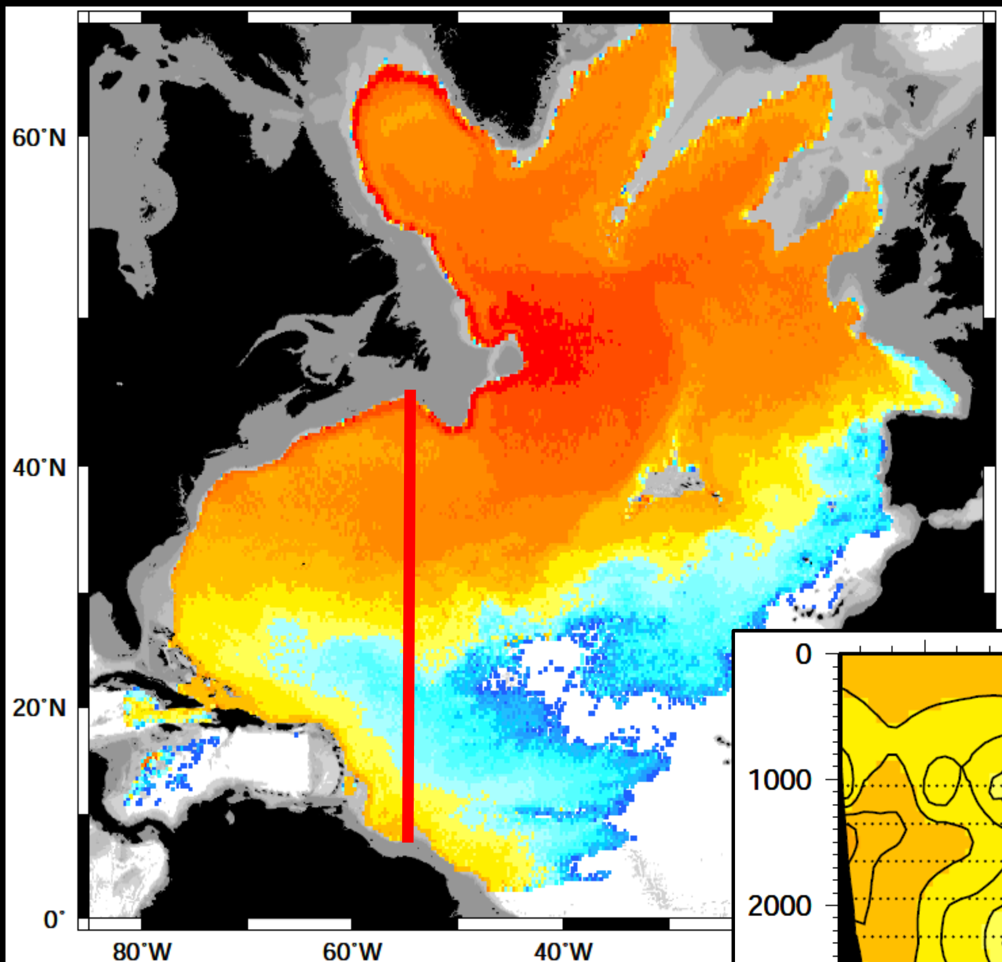

Standard deviation of age of Lagrangian particles in each ¼° x ¼° grid box over 50 year simulation [years]

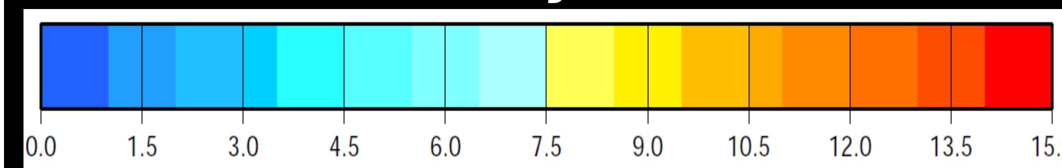

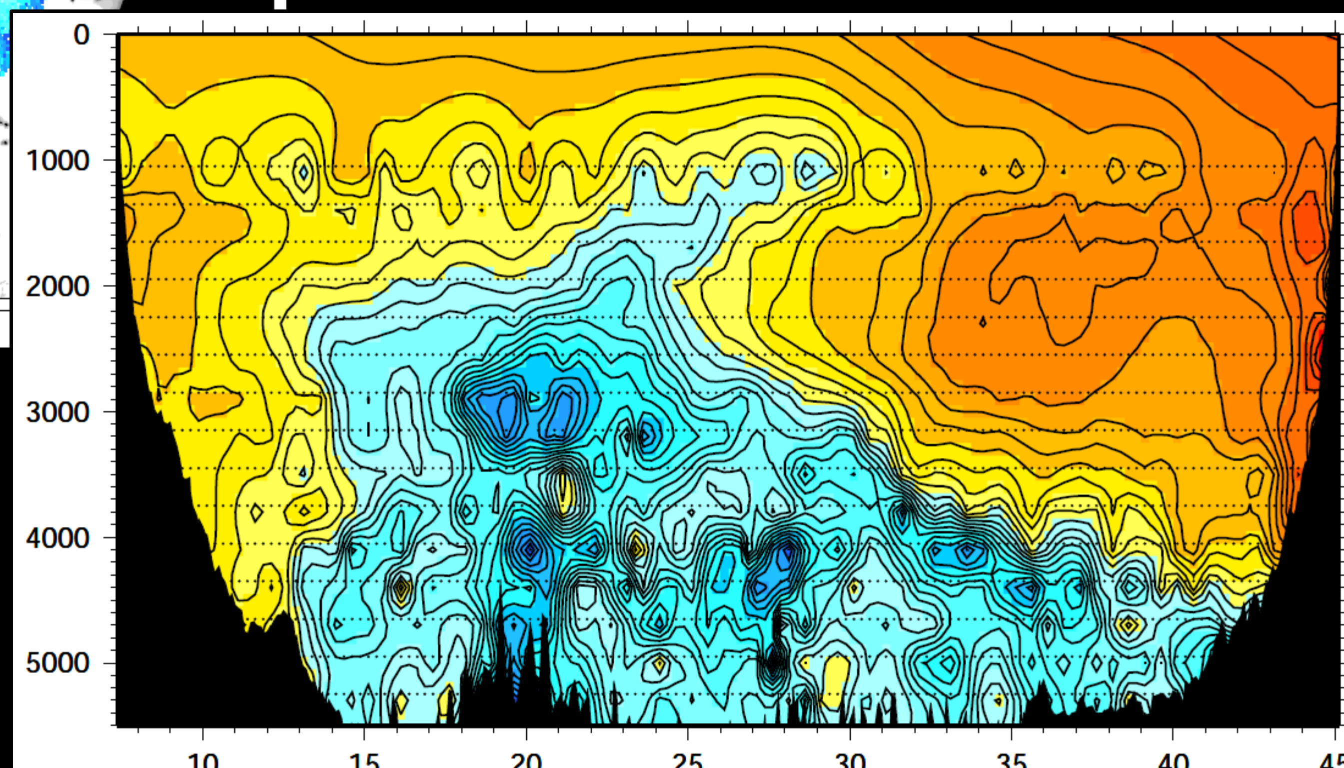

Conclusions

(1) Both observations and models exhibit:
- Stable Deep Western Boundary Current
- High CFC-11 concentration DWBC core
- Rapid exit of particles from the DWBC

(2) Modeled DWBC tracer signal propagation is similar to observations.

(3) Simulated Lagrangian particles reproduce the observed spreading pathways of LSW and tracer.

(4) The interior pathway, identified by simulated Lagrangian pathways, is consistent with tracer and float observations. This pathway exports a significant amount of LSW.

References

Barnier, B. et al. 2006. Impact of partial steps and momentum advection schemes in a global ocean circulation model at eddy permitting resolution. Oce. Dyn. (56) pp. 543-567.

Blanke, B. and N. Grima. 2010. ARIANE v2.2.6 Laboratoire de Physique des Oceans. http://stockage.univ-brest.fr/~grima/Ariane/

Bower, A. S., M. S. Lozier, S. F. Gary, and C. W. Böning. 2009. Interior pathways of the North Atlantic Meridional Overturning Circulation. Nature (459) pp. 243-247.

Doney, S. C. and W. J. Jenkins. 1994. Ventilation of the DWBC and the abyssal western North Atlantic: Estimates from tritium and ^{3}He distributions. JPO (24) pp. 638-659.

Fischer, J. and F. A. Schott. 2002. Labrador Sea Water tracked by profiling floats – From the boundary current to the open North Atlantic. JPO (32) pp. 572-584.

Lavender, K. L., R. E. Davis, and W. B. Owens. 2000. Mid-depth recirculation observed in the interior Labrador and Irminger Seas by direct velocity measurements. Nature (407) pp. 66-69.

CARINA group. 2009. Carbon in the Atlantic Ocean Region – the CARINA project: Results and Data, Version 1.0. http://cdiac.ornl.gov/ftp/oceans/CARINA/CARINA_Database/CARINA.ATL.V1.0/ Carbon Dioxide Information Analysis Center, Oak Ridge National Laboratory, U.S. Department of Energy, Oak Ridge, Tennessee. doi:10.3334/CDIAC/otg.CARINA.ATL.V1.0

Key, R. M., A. Kozyr, C. L. Sabine, K. Lee, R. Wanninkhof, J. L. Bullister, R. A. Feely, F. J. Millero, C. Mordy, and T.-H. Peng (2004), A global ocean carbon climatology: Results from Global Data Analysis Project (GLODAP), *Global Biogeochemical Cycles*, 18, GB4031, doi:10.1029/2004GB002247.

Large, W. G. and S. G. Yeager. 2004. Dirunal to decadal global forcing for ocean and sea-ice models: the data sets and flux climatologies. NCAR Technical Note NCAR/TN-460+STR. National Center for Atmospheric Research, Boulder, CO.

Schott, F. et al. 2004. Circulation and deep water export at the western exit of the subpolar North Atlantic. JPO (34) pp. 817-843.

Schott, F. et al. 2006. Variability of the DWBC east of the Grand Banks. GRL (33) L21S07, doi:10.1029/2006GL026563.

Smethie, W. M. 1993. Tracing the thermohaline circulation in the western North Atlantic using chlorofluorocarbons. Prog. Oce.(31) pp. 51-99.

Smethie, W. M. et al. 2000. Tracing the flow of North Atlantic deep water using chlorofluorocarbons. JGR(105) pp. 14297-14323.

Stommel, H. 1958. The abyssal circulation. Deep Sea Research (5) pp. 80-82.

Talley, L. T., M. S. McCartney. 1982. Distribution and Circulation of Labrador Sea Water. JPO (12) pp. 1189-1205.

Watts, D. R. 1991. Equatorward currents in temperatures 1.8-6.0ºCon the continental slope in the Mid-Atlantic Bight, in: P. C. Chu and J.C. Gascard (Eds.), Deep Convection and Deep Water Formation in the Oceans. Elsevier, Amsterdam, pp. 183-196.

Observed and modeled CFC11 at 44ºN

CARINA #12, Oct-Nov 1994

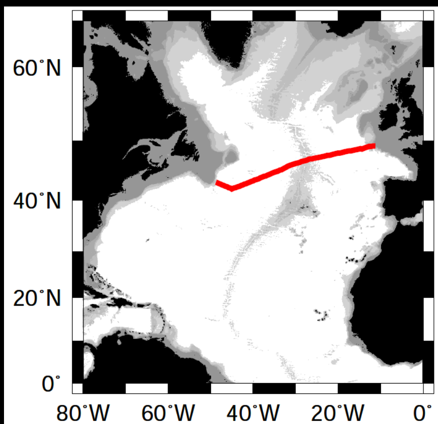

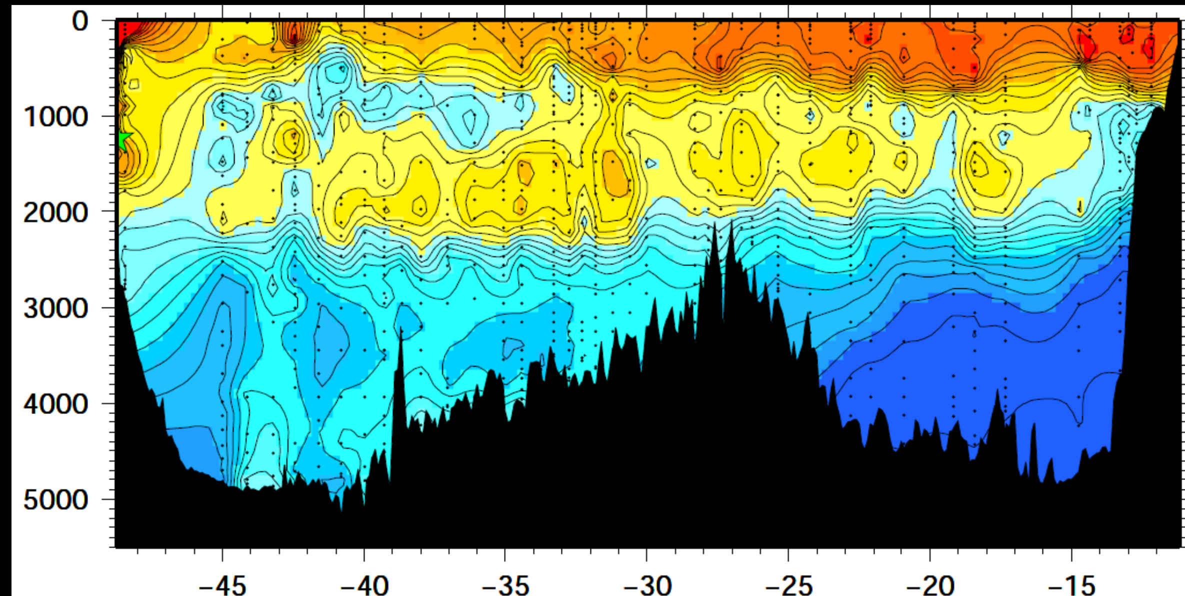

ORCA025, Oct. mean 1994

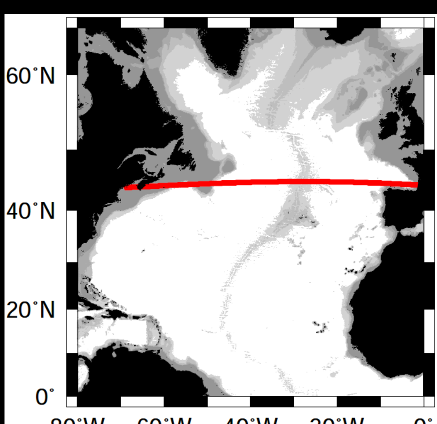

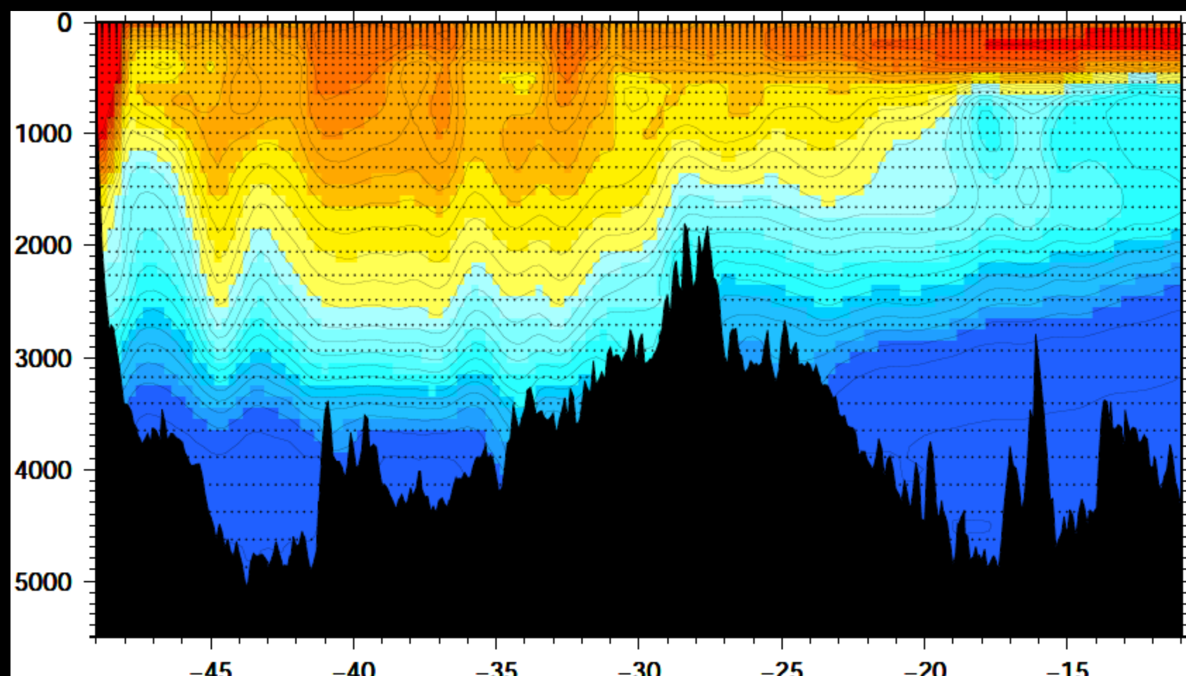

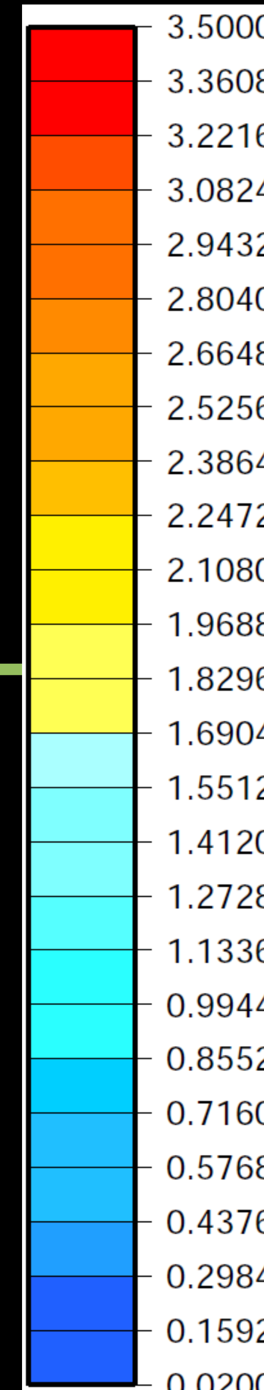

Probability distribution

Probability of Lagrangian particle in each ¼° x ¼° grid box over 50 year simulation.

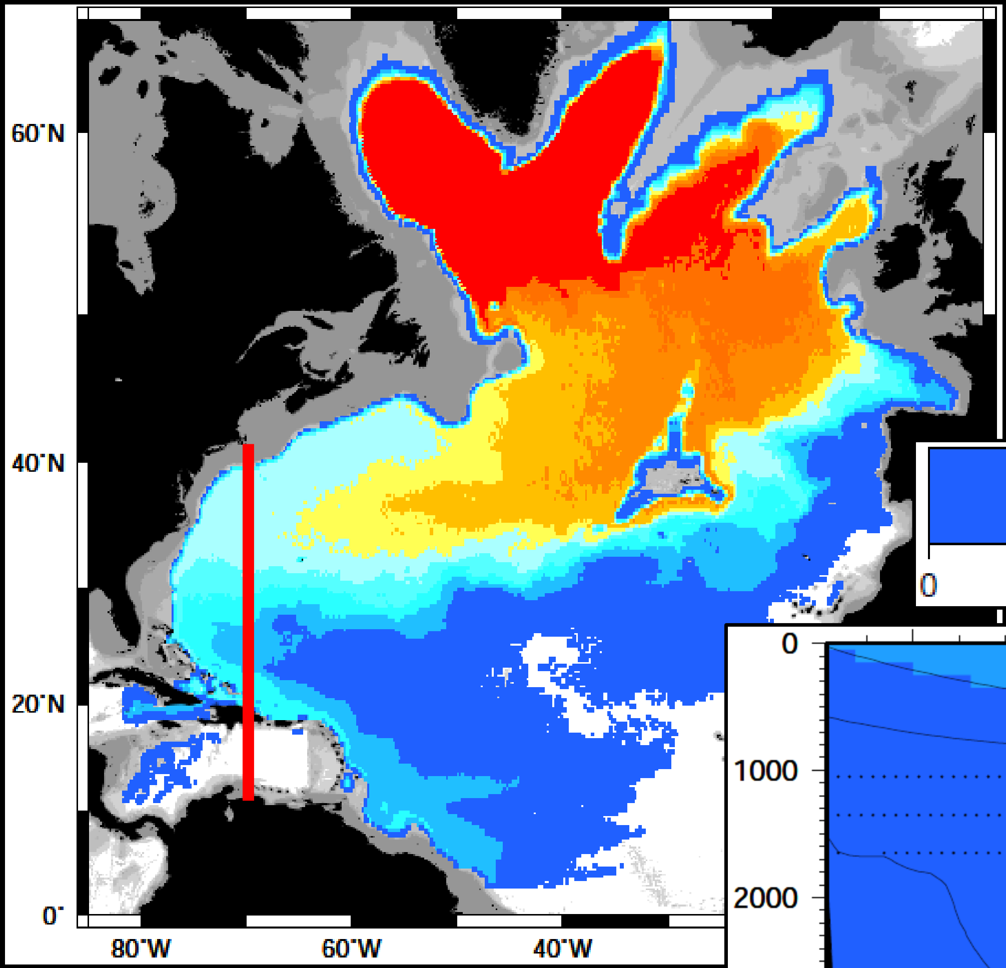

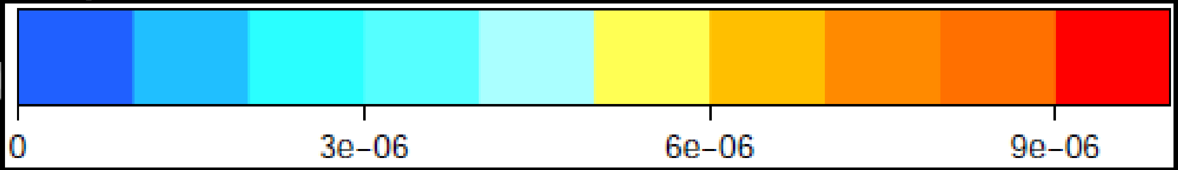

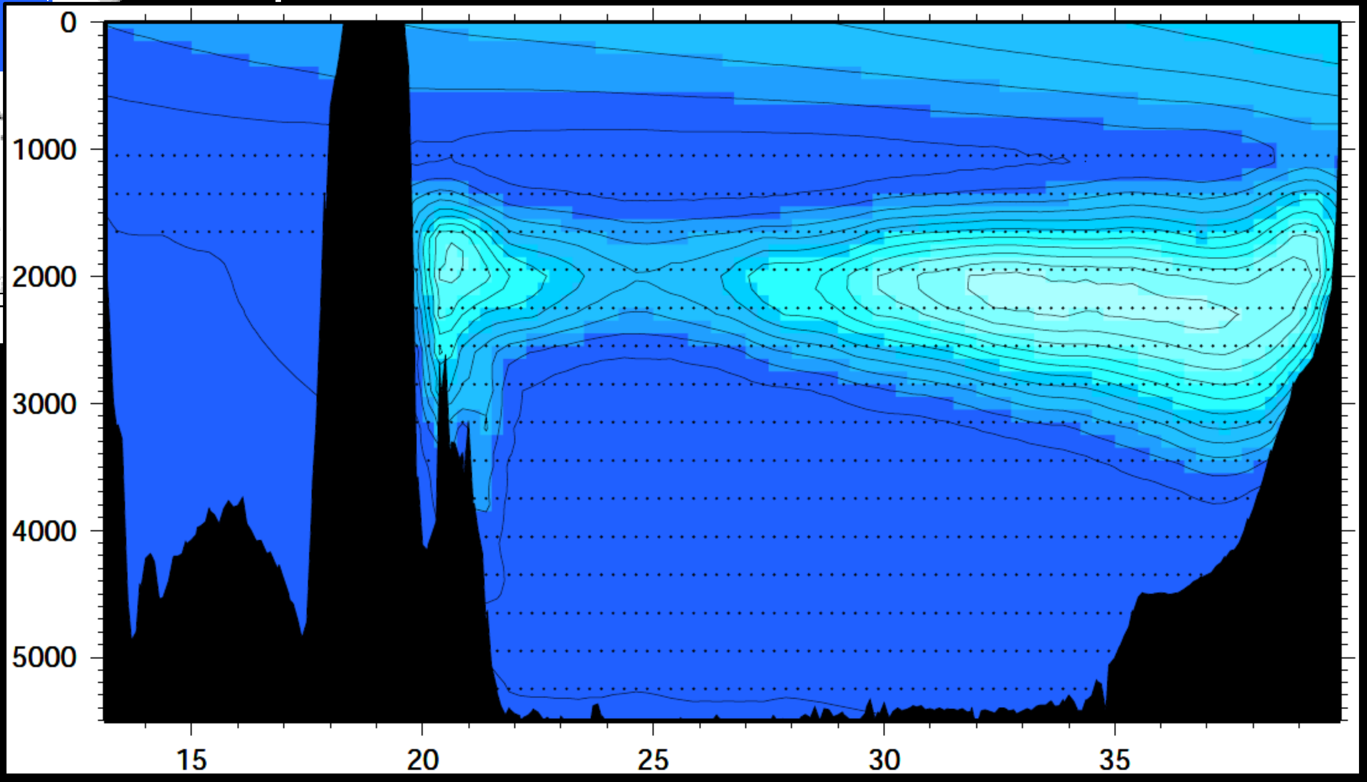

Age distribution

Average age of Lagrangian particles in each ¼° x ¼° grid box over 50 year simulation [years]

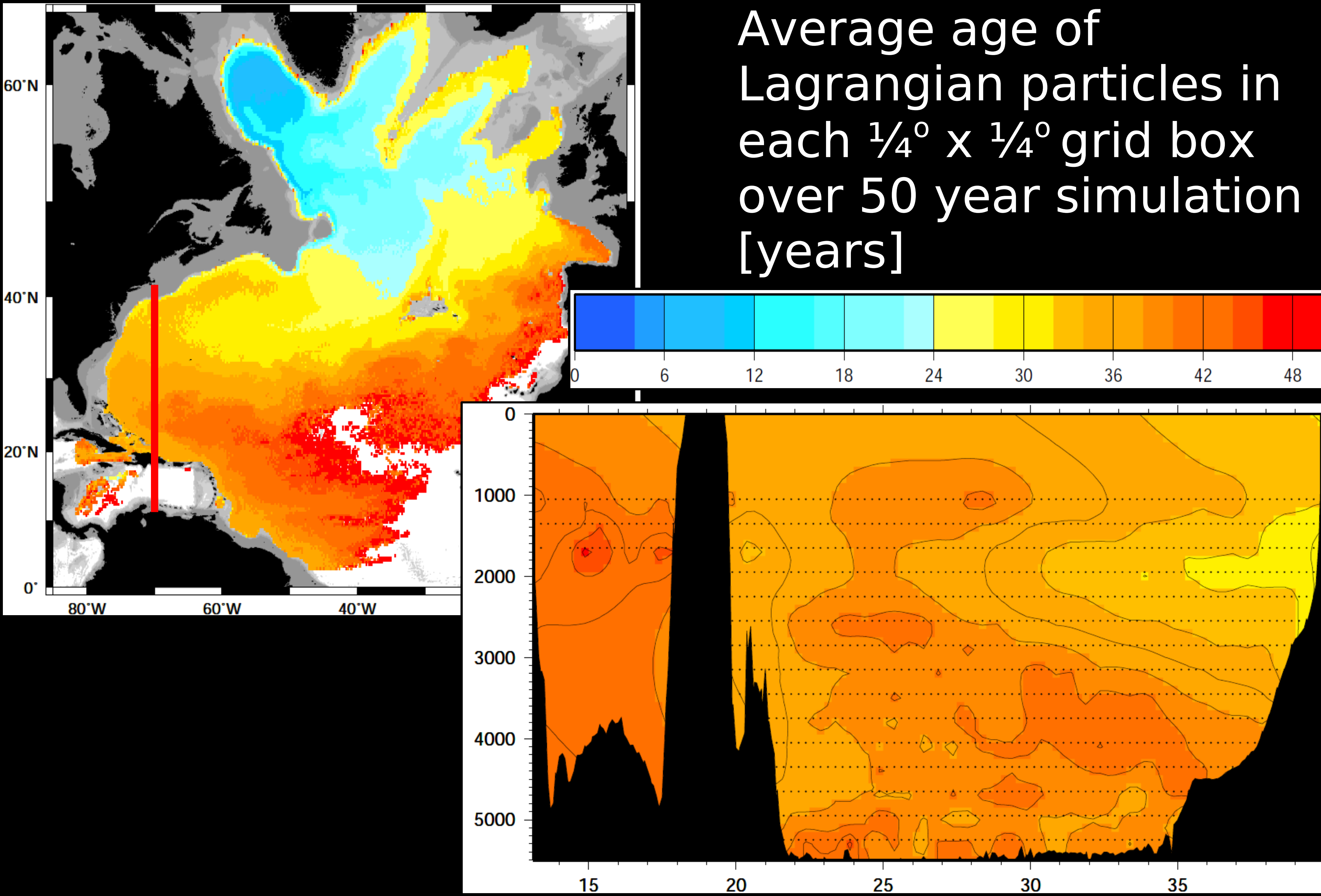

Age distribution

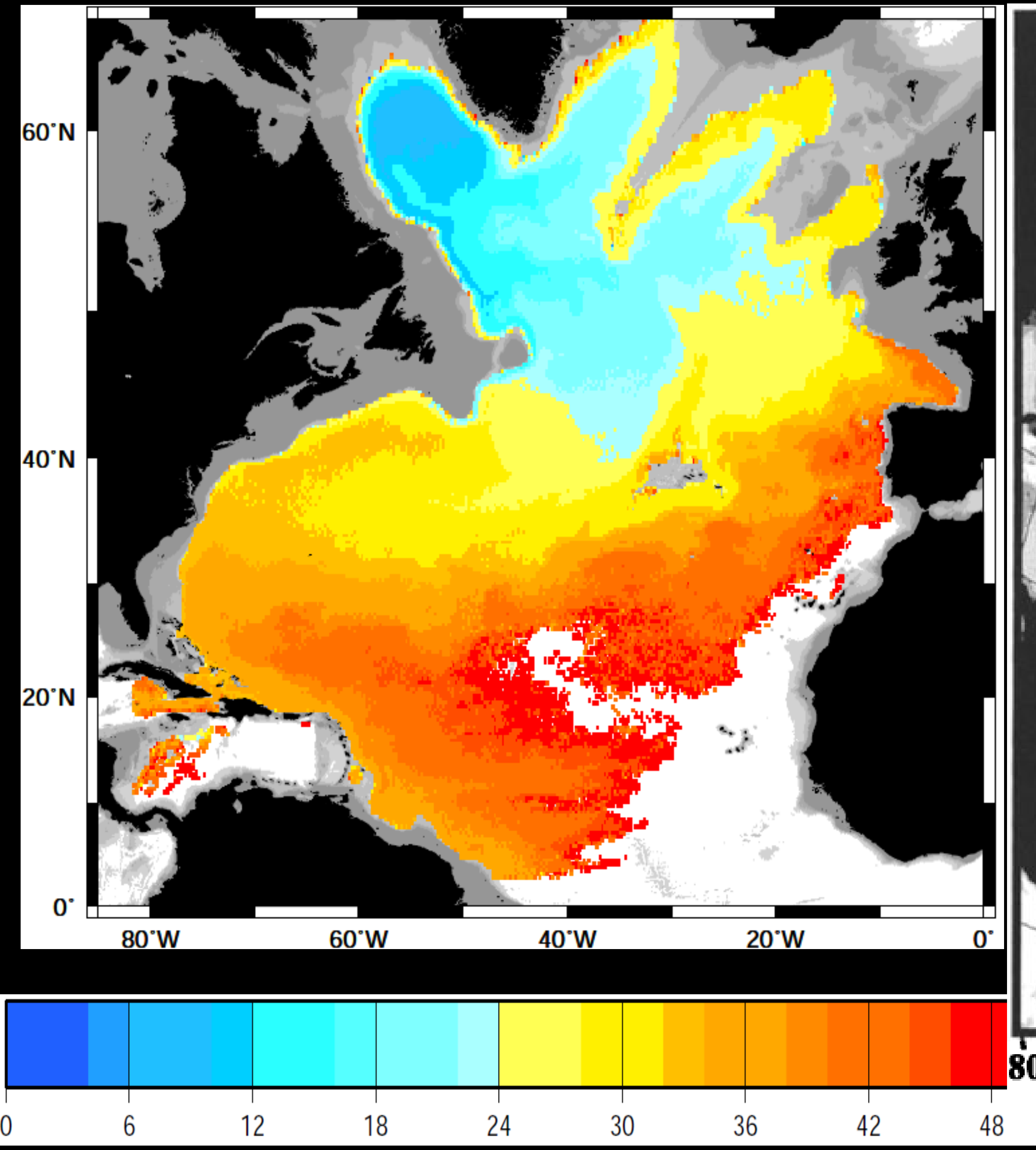

Average Lagrangian age [years]

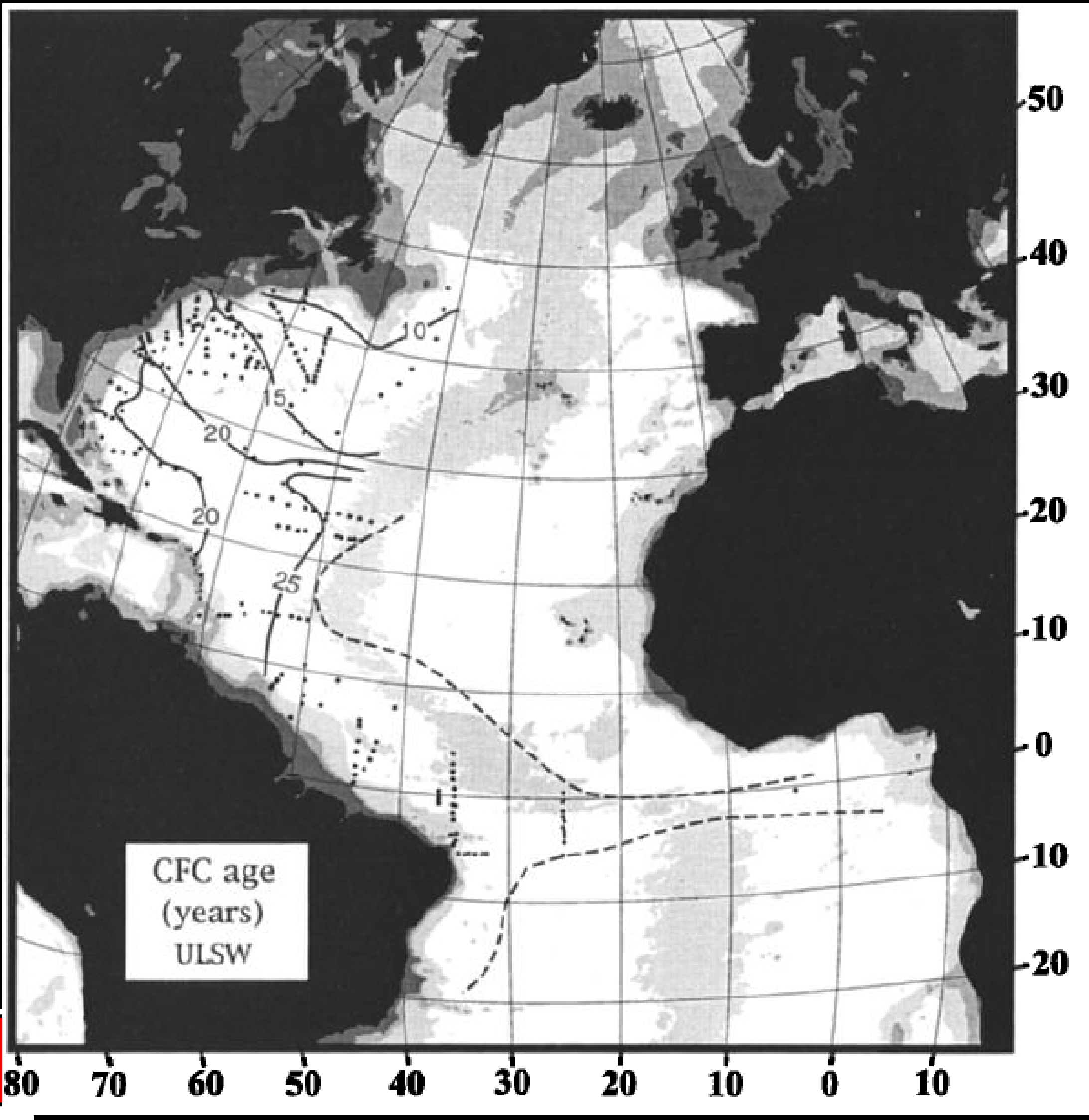

CFC-11/CFC-12 ratio age [years] (Smethie et al., 2000)

Variability in the age distribution

Standard deviation of age of Lagrangian particles in each ¼° x ¼° grid box over 50 year simulation.

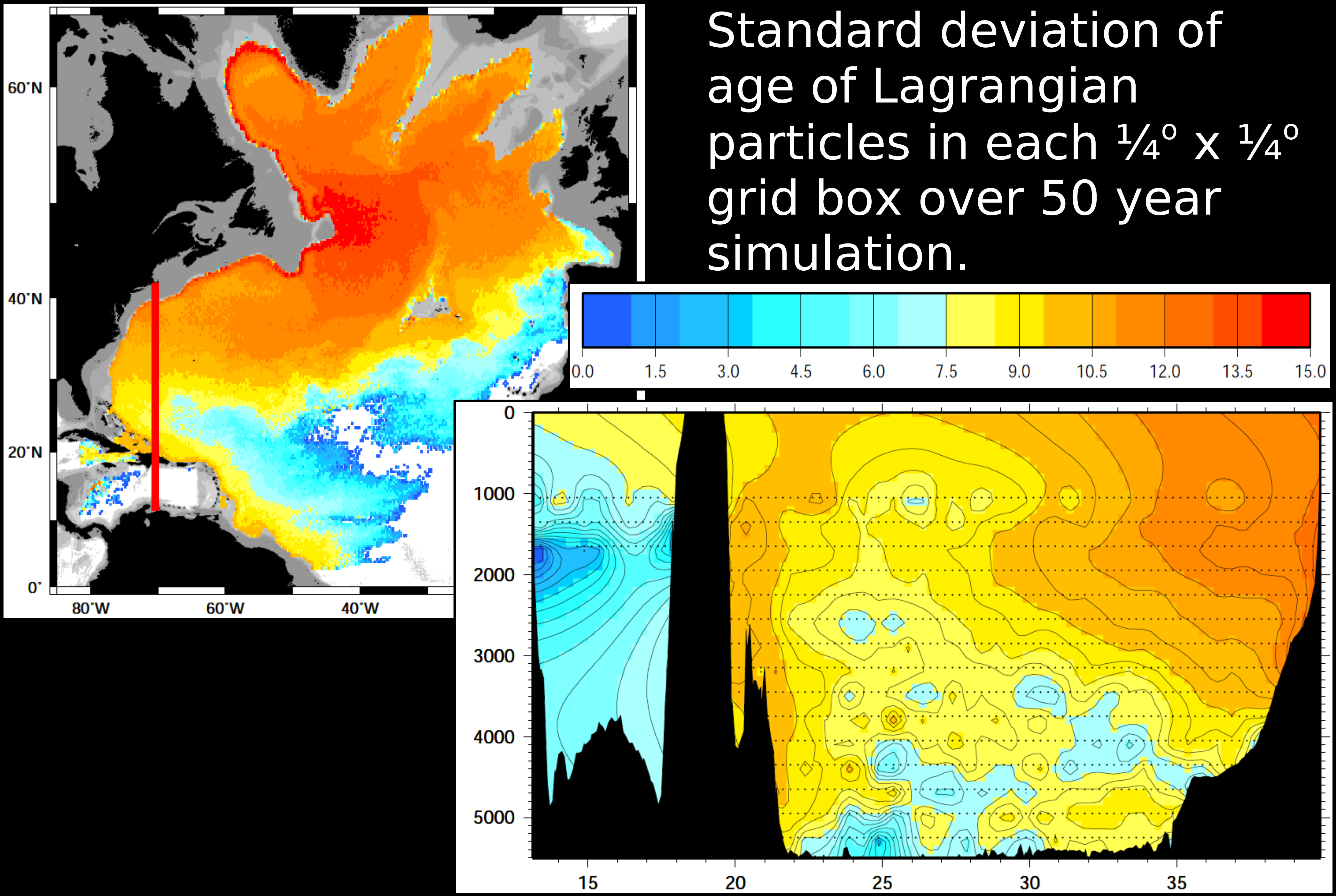

Connectivity of the Lagrangian signal

ORCA025 Float probability max inshore below 1000m